The 12th KIAS Workshop on Particle Physics and Cosmology and 2024 Korea-France STAR workshop, 2024.11.18. KIAS

Probing the Heavy Dark Z' at multi-TeV muon colliders

Jeonghyeon Song (Konkuk University, Korea)

With J.Kim, S.Lee, P.Sanyal, and K.Cheung

I. Motivation for the Dark Sector

II. Dark Photon

III. Multi-TeV Muon Collider

IV. Dark Z at the MuC

V. Signal-to-Background analysis

VI. Conclusions

I. Motivation for the Dark Sector

No hints for BSM at the LHC

ATLAS Exotics Searches* - 95% CL Upper Exclusion Limits

Status: May 2019

ATLAS Preliminary

$\int \mathcal{L}\, dt$ = (3.2 – 139) fb^{-1} $\sqrt{s}$ = 8, 13 TeV

	Model	ℓ, γ	Jets†	E_T^{miss}	$\int \mathcal{L}\, dt$[fb^{-1}]	Limit		Reference
Extra dimensions	ADD $G_{KK} + g/q$	0 e, μ	1 – 4 j	Yes	36.1	M_D 7.7 TeV	$n = 2$	1711.03301
	ADD non-resonant $\gamma\gamma$	2 γ	–	–	36.7	M_S 8.6 TeV	$n = 3$ HLZ NLO	1707.04147
	ADD QBH	–	2 j	–	37.0	M_{th} 8.9 TeV	$n = 6$	1703.09127
	ADD BH high $\sum p_T$	≥ 1 e, μ	≥ 2 j	–	3.2	M_{th} 8.2 TeV	$n = 6$, $M_D = 3$ TeV, rot BH	1606.02265
	ADD BH multijet	–	≥ 3 j	–	3.6	M_{th} 9.55 TeV	$n = 6$, $M_D = 3$ TeV, rot BH	1512.02586
	RS1 $G_{KK} \to \gamma\gamma$	2 γ	–	–	36.7	G_{KK} mass 4.1 TeV	$k/\overline{M}_{Pl} = 0.1$	1707.04147
	Bulk RS $G_{KK} \to WW/ZZ$	multi-channel			36.1	G_{KK} mass 2.3 TeV	$k/\overline{M}_{Pl} = 1.0$	1808.02380
	Bulk RS $G_{KK} \to WW \to qqqq$	0 e, μ	2 J	–	139	G_{KK} mass 1.6 TeV	$k/\overline{M}_{Pl} = 1.0$	ATLAS-CONF-2019-003
	Bulk RS $g_{KK} \to tt$	1 e, μ	≥ 1 b, ≥ 1J/2j	Yes	36.1	g_{KK} mass 3.8 TeV	$\Gamma/m = 15\%$	1804.10823
	2UED / RPP	1 e, μ	≥ 2 b, ≥ 3 j	Yes	36.1	KK mass 1.8 TeV	Tier (1,1), $\mathcal{B}(A^{(1,1)} \to tt) = 1$	1803.09678
Gauge bosons	SSM $Z' \to \ell\ell$	2 e, μ	–	–	139	Z' mass 5.1 TeV		1903.06248
	SSM $Z' \to \tau\tau$	2 τ	–	–	36.1	Z' mass 2.42 TeV		1709.07242
	Leptophobic $Z' \to bb$	–	2 b	–	36.1	Z' mass 2.1 TeV		1805.09299
	Leptophobic $Z' \to tt$	1 e, μ	≥ 1 b, ≥ 1J/2j	Yes	36.1	Z' mass 3.0 TeV	$\Gamma/m = 1\%$	1804.10823
	SSM $W' \to \ell\nu$	1 e, μ	–	Yes	139	W' mass 6.0 TeV		CERN-EP-2019-100
	SSM $W' \to \tau\nu$	1 τ	–	Yes	36.1	W' mass 3.7 TeV		1801.06992
	HVT $V' \to WZ \to qqqq$ model B	0 e, μ	2 J	–	139	V' mass 3.6 TeV	$g_V = 3$	ATLAS-CONF-2019-003
	HVT $V' \to WH/ZH$ model B	multi-channel			36.1	V' mass 2.93 TeV	$g_V = 3$	1712.06518
	LRSM $W_R \to tb$	multi-channel			36.1	W_R mass 3.25 TeV		1807.10473
	LRSM $W_R \to \mu N_R$	2 μ	1 J	–	80	W_R mass 5.0 TeV	$m(N_R) = 0.5$ TeV, $g_L = g_R$	1904.12679
CI	CI $qqqq$	–	2 j	–	37.0	Λ 21.8 TeV	η_{LL}^-	1703.09127
	CI $\ell\ell qq$	2 e, μ	–	–	36.1	Λ 40.0 TeV	η_{LL}^-	1707.02424
	CI $tttt$	≥1 e, μ	≥1 b, ≥1 j	Yes	36.1	Λ 2.57 TeV	$\lvert C_{4t} \rvert = 4\pi$	1811.02305
DM	Axial-vector mediator (Dirac DM)	0 e, μ	1 – 4 j	Yes	36.1	m_{med} 1.55 TeV	g_q=0.25, g_χ=1.0, $m(\chi) = 1$ GeV	1711.03301
	Colored scalar mediator (Dirac DM)	0 e, μ	1 – 4 j	Yes	36.1	m_{med} 1.67 TeV	g=1.0, $m(\chi) = 1$ GeV	1711.03301
	$VV\chi\chi$ EFT (Dirac DM)	0 e, μ	1 J, ≤ 1 j	Yes	3.2	M_* 700 GeV	$m(\chi) < 150$ GeV	1608.02372
	Scalar reson. $\phi \to t\chi$ (Dirac DM)	0-1 e, μ	1 b, 0-1 J	Yes	36.1	m_ϕ 3.4 TeV	$y = 0.4$, $\lambda = 0.2$, $m(\chi) = 10$ GeV	1812.09743
LQ	Scalar LQ 1st gen	1,2 e	≥ 2 j	Yes	36.1	LQ mass 1.4 TeV	$\beta = 1$	1902.00377
	Scalar LQ 2nd gen	1,2 μ	≥ 2 j	Yes	36.1	LQ mass 1.56 TeV	$\beta = 1$	1902.00377
	Scalar LQ 3rd gen	2 τ	2 b	–	36.1	LQ_3^u mass 1.03 TeV	$\mathcal{B}(LQ_3^u \to b\tau) = 1$	1902.08103
	Scalar LQ 3rd gen	0-1 e, μ	2 b	Yes	36.1	LQ_3^d mass 970 GeV	$\mathcal{B}(LQ_3^d \to t\tau) = 0$	1902.08103
Heavy quarks	VLQ $TT \to Ht/Zt/Wb + X$	multi-channel			36.1	T mass 1.37 TeV	SU(2) doublet	1808.02343
	VLQ $BB \to Wt/Zb + X$	multi-channel			36.1	B mass 1.34 TeV	SU(2) doublet	1808.02343
	VLQ $T_{5/3}\,T_{5/3} \lvert T_{5/3} \to Wt + X$	2(SS)/≥3 e, μ	≥1 b, ≥1 j	Yes	36.1	$T_{5/3}$ mass 1.64 TeV	$\mathcal{B}(T_{5/3} \to Wt) = 1$, $c(T_{5/3}Wt) = 1$	1807.11883
	VLQ $Y \to Wb + X$	1 e, μ	≥ 1 b, ≥ 1j	Yes	36.1	Y mass 1.85 TeV	$\mathcal{B}(Y \to Wb) = 1$, $c_R(Wb) = 1$	1812.07343
	VLQ $B \to Hb + X$	0 e, μ, 2 γ	≥ 1 b, ≥ 1j	Yes	79.8	B mass 1.21 TeV	$\kappa_B = 0.5$	ATLAS-CONF-2018-024
	VLQ $QQ \to WqWq$	1 e, μ	≥ 4 j	Yes	20.3	Q mass 690 GeV		1509.04261
Excited fermions	Excited quark $q^* \to qg$	–	2 j	–	139	q^* mass 6.7 TeV	only u^* and d^*, $\Lambda = m(q^*)$	ATLAS-CONF-2019-007
	Excited quark $q^* \to q\gamma$	1 γ	1 j	–	36.7	q^* mass 5.3 TeV	only u^* and d^*, $\Lambda = m(q^*)$	1709.10440
	Excited quark $b^* \to bg$	–	1 b, 1 j	–	36.1	b^* mass 2.6 TeV		1805.09299
	Excited lepton ℓ^*	3 e, μ	–	–	20.3	ℓ^* mass 3.0 TeV	$\Lambda = 3.0$ TeV	1411.2921
	Excited lepton ν^*	3 e, μ, τ	–	–	20.3	ν^* mass 1.6 TeV	$\Lambda = 1.6$ TeV	1411.2921
Other	Type III Seesaw	1 e, μ	≥ 2 j	Yes	79.8	N^0 mass 560 GeV		ATLAS-CONF-2018-020
	LRSM Majorana ν	2 μ	2 j	–	36.1	N_R mass 3.2 TeV	$m(W_R) = 4.1$ TeV, $g_L = g_R$	1809.11105
	Higgs triplet $H^{\pm\pm} \to \ell\ell$	2,3,4 e, μ (SS)	–	–	36.1	$H^{\pm\pm}$ mass 870 GeV	DY production	1710.09748
	Higgs triplet $H^{\pm\pm} \to \ell\tau$	3 e, μ, τ	–	–	20.3	$H^{\pm\pm}$ mass 400 GeV	DY production, $\mathcal{B}(H_L^{\pm\pm} \to \ell\tau) = 1$	1411.2921
	Multi-charged particles	–	–	–	36.1	multi-charged particle mass 1.22 TeV	DY production, $\lvert q \rvert = 5e$	1812.03673
	Magnetic monopoles	–	–	–	34.4	monopole mass 2.37 TeV	DY production, $\lvert g \rvert = 1g_D$, spin 1/2	1905.10130

$\sqrt{s}$ = 8 TeV | $\sqrt{s}$ = 13 TeV partial data | $\sqrt{s}$ = 13 TeV full data

10^{-1} 1 10 **Mass scale [TeV]**

**Only a selection of the available mass limits on new states or phenomena is shown.*

†Small-radius (large-radius) jets are denoted by the letter j (J).

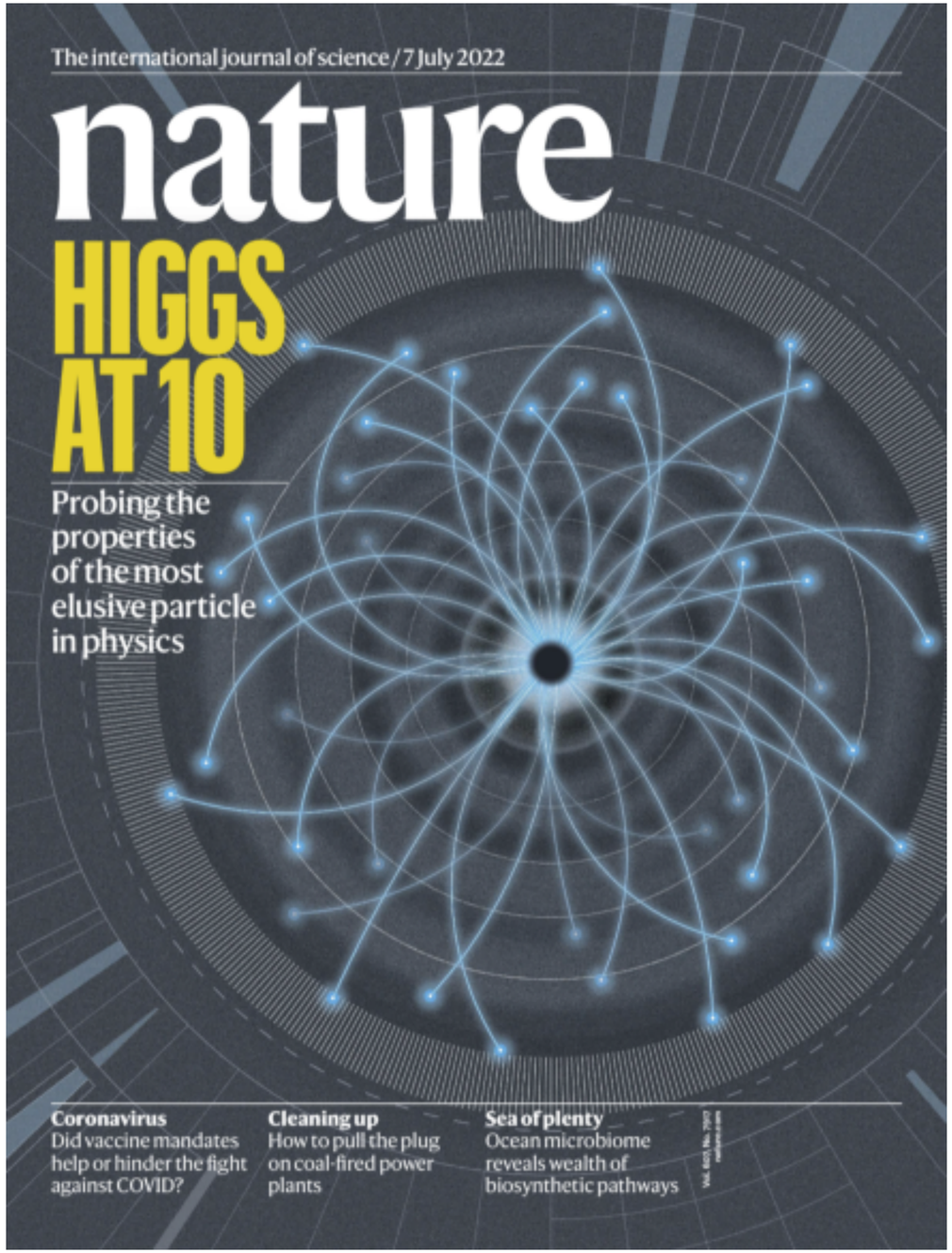

Article

A detailed map of Higgs boson interactions by the ATLAS experiment ten years after the discovery

https://doi.org/10.1038/s41586-022-04893-w

The ATLAS Collaboration*✉

Article

A portrait of the Higgs boson by the CMS experiment ten years after the discovery

https://doi.org/10.1038/s41586-022-04892-x

The CMS Collaboration*✉

Received: 21 March 2022

Production

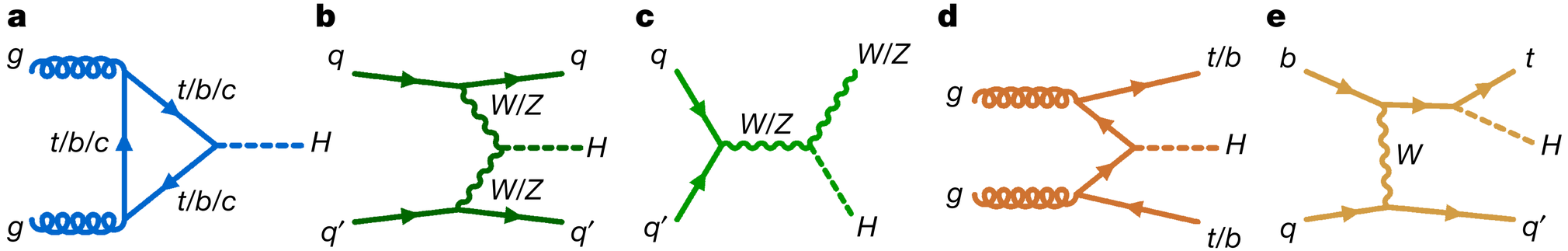

Decay

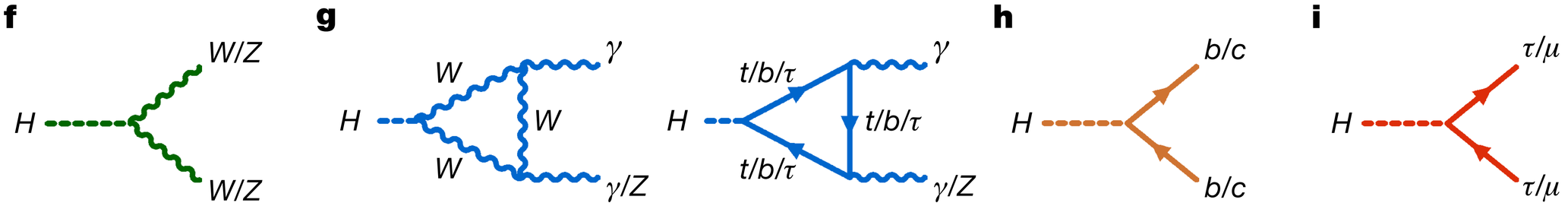

Production

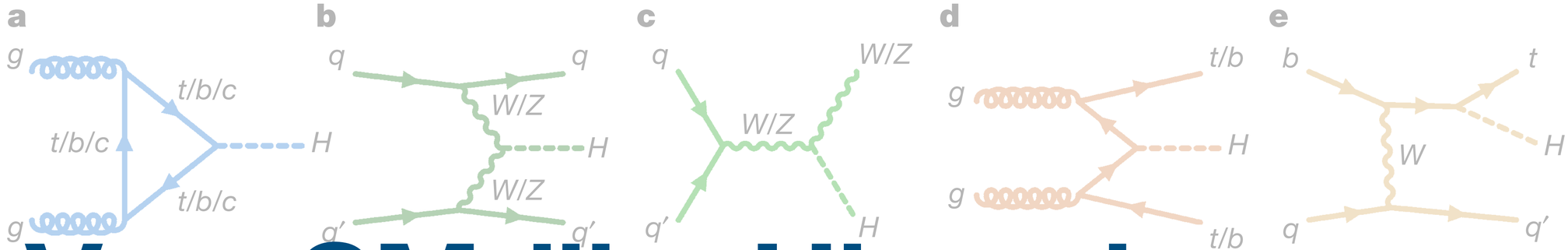

Very SM-like Higgs boson

Decay

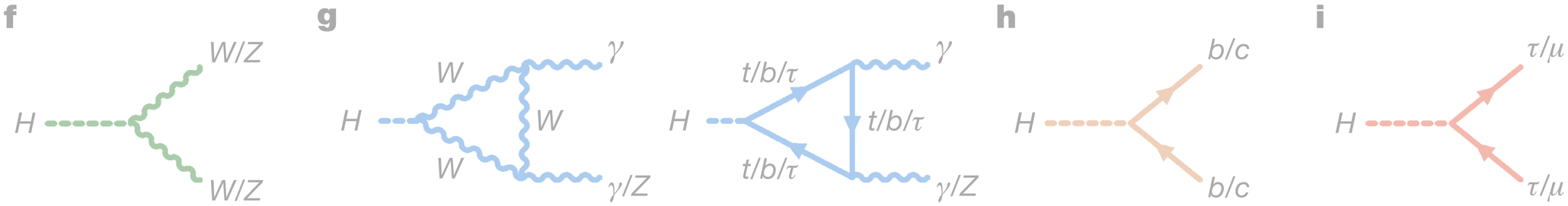

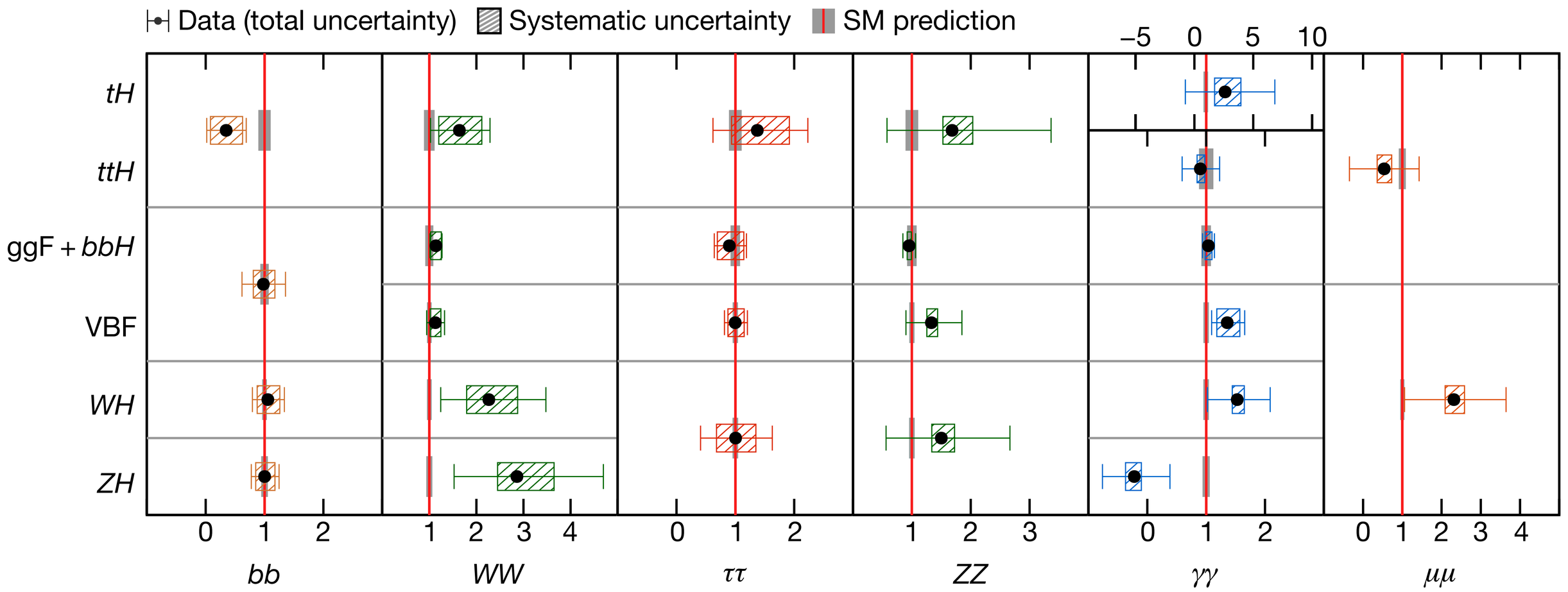
Data (total uncertainty)
Systematic uncertainty
SM prediction
tH
ttH
ggF + bbH
VBF
WH
ZH
bb
WW
ττ
ZZ
γγ
μμ

Editors' Suggestion | Featured in Physics

Evidence for the Higgs Boson Decay to a Z Boson and a Photon at the LHC

G. Aad *et al.*[*]
(ATLAS and CMS Collaborations)

(Received 8 September 2023; accepted 27 November 2023; published 11 January 2024)

The first evidence for the Higgs boson decay to a Z boson and a photon is presented, with a statistical significance of 3.4 standard deviations. The result is derived from a combined analysis of the searches performed by the ATLAS and CMS Collaborations with proton-proton collision datasets collected at the CERN Large Hadron Collider (LHC) from 2015 to 2018. These correspond to integrated luminosities of around 140 fb^{-1} for each experiment, at a center-of-mass energy of 13 TeV. The measured signal yield is 2.2 ± 0.7 times the standard model prediction, and agrees with the theoretical expectation within 1.9 standard deviations.

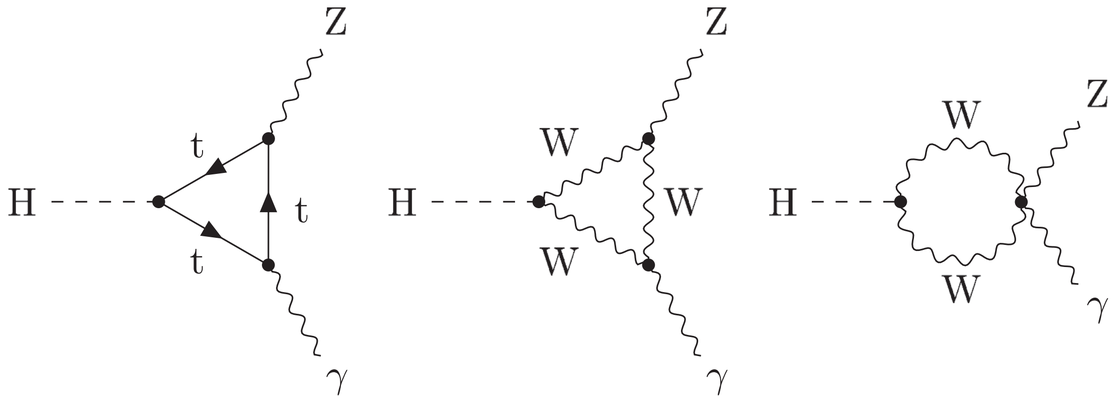

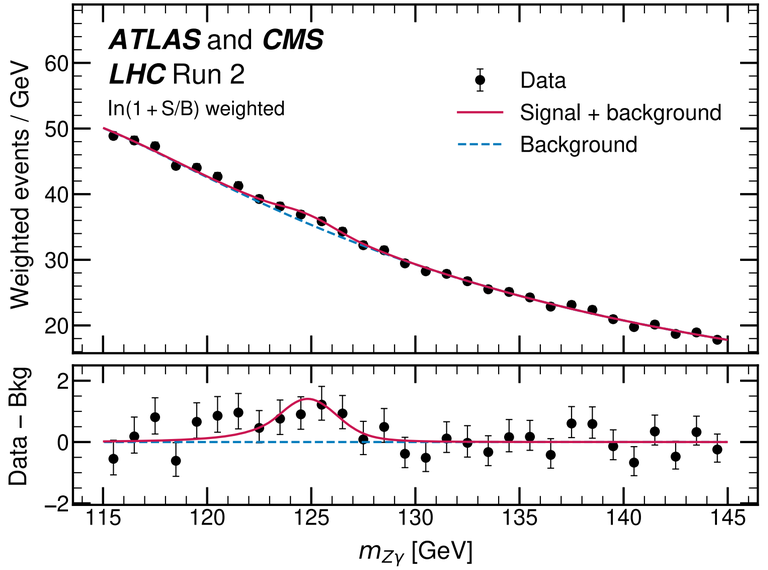

One possible answer: Dark Sector

(1) Not charged under the Standard Model gauge groups

(2) No new particles have been seen simply because they do not interact through the Standard Model gauge interactions.

(3) We need a portal to observe particles belong to the dark sector.

Best candidates for the portal particle

- Dark photon (or Dark Z)
- Neutrino (spin 1/2)
- Dark Higgs (scalar)
- Axion (pseudo-scalar).

Best candidates for the portal particle

- Dark photon (or Dark Z)
- Neutrino (spin 1/2)
- Dark Higgs (scalar)
- Axion (pseudo-scalar).


Dark Z

II. Dark Photon

Basic Lagrangian

- Two gauge group $U(1)_a$ and $U(1)_b$

$$\mathcal{L}_0 = -\frac{1}{4} F_{a\mu\nu} F_a^{\mu\nu} - \frac{1}{4} F_{b\mu\nu} F_b^{\mu\nu} - \frac{\varepsilon}{2} F_{a\mu\nu} F_b^{\mu\nu} \,.$$

- Coupling to the SM current J_μ and the dark sector current J'_μ

$$\mathcal{L} = e\, J_\mu A_b^\mu + e'\, J'_\mu A_a^\mu$$

- Two cases: massless dark photon and massive dark photon ➡ very different

Massless dark photon: diagonalization

- Diagonalize the kinetic terms

$$\begin{pmatrix} A_a^\mu \\ A_b^\mu \end{pmatrix} = \begin{pmatrix} \dfrac{1}{\sqrt{1-\varepsilon^2}} & 0 \\ -\dfrac{\varepsilon}{\sqrt{1-\varepsilon^2}} & 1 \end{pmatrix} \begin{pmatrix} \cos\theta & -\sin\theta \\ \sin\theta & \cos\theta \end{pmatrix} \begin{pmatrix} A'^\mu \\ A^\mu \end{pmatrix}$$

Dark photon

SM photon

- θ ➡ Arbitrary as long as the gauge bosons are massless.

Massless dark photon: freedom

- Interaction Lagrangian

$$\begin{aligned}\mathcal{L}' &= \left[\frac{e'\cos\theta}{\sqrt{1-\varepsilon^2}}J'_\mu + e\left(\sin\theta - \frac{\varepsilon\cos\theta}{\sqrt{1-\varepsilon^2}}\right)J_\mu\right]A'^\mu \\ &+ \left[-\frac{e'\sin\theta}{\sqrt{1-\varepsilon^2}}J'_\mu + e\left(\cos\theta + \frac{\varepsilon\sin\theta}{\sqrt{1-\varepsilon^2}}\right)J_\mu\right]A^\mu .\end{aligned}$$

- Freedom!

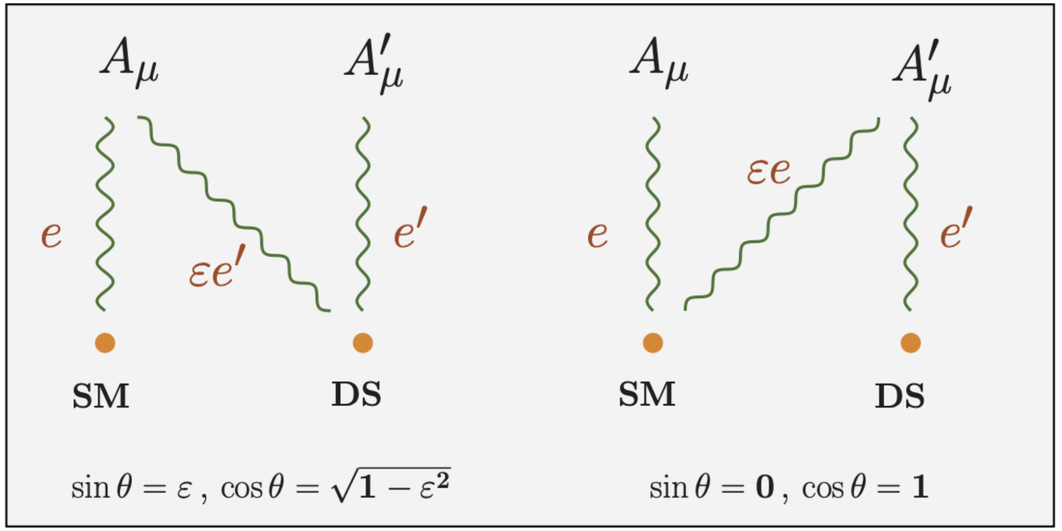

Massive dark photon

(1) The diagonalization of the mass terms determines θ.

(2) Mass terms? Stueckelberg Lagrangian or Dark Higgs

(3) Question: Which kinetic mixing?

Electric or hyper-charge?

(4) The answer depends on the dark photon mass scale

Current Bounds on the Dark Photon

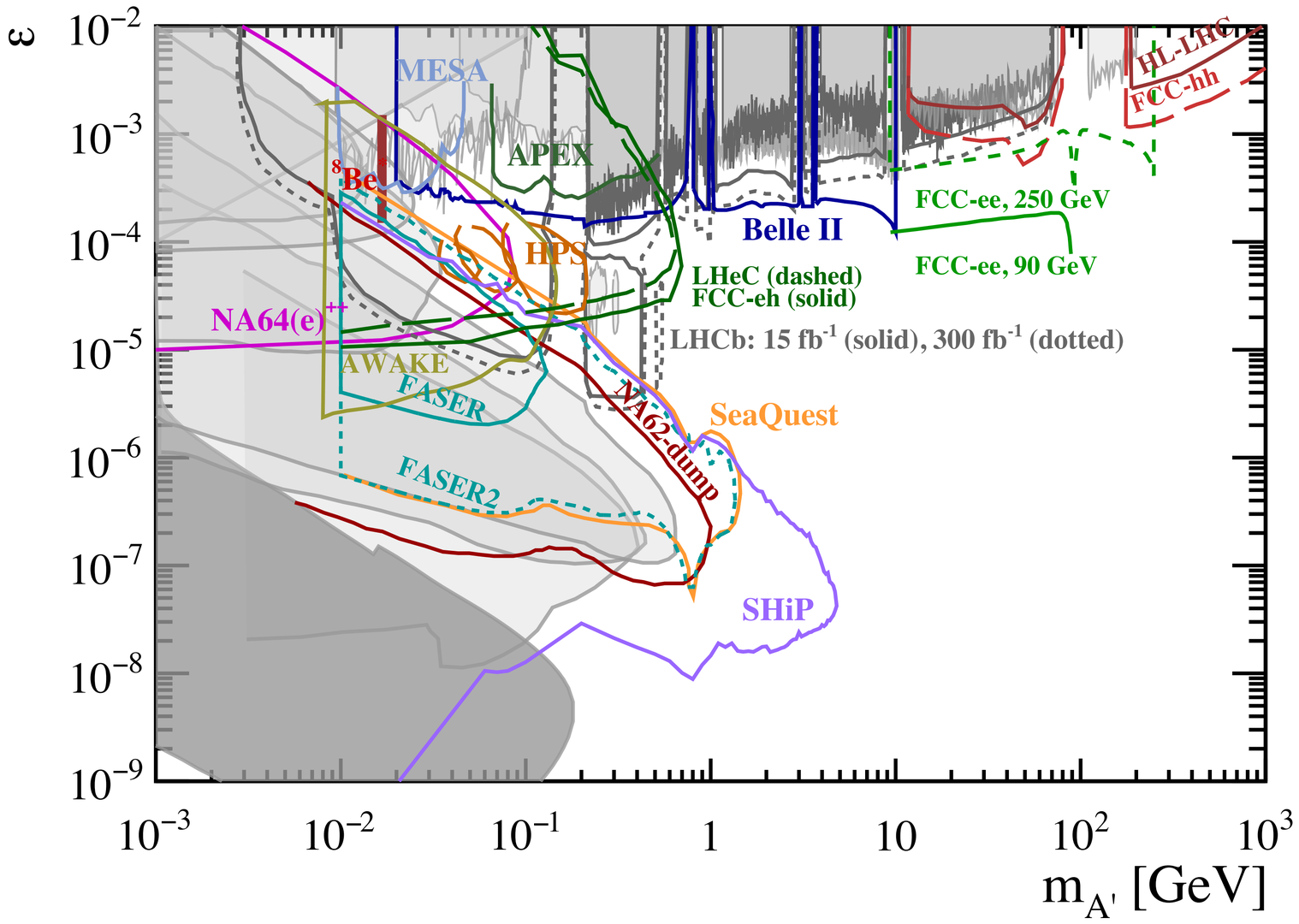

[2005.01515]

Almost excluded for $m'_A < 0.1\,\mathrm{GeV}$

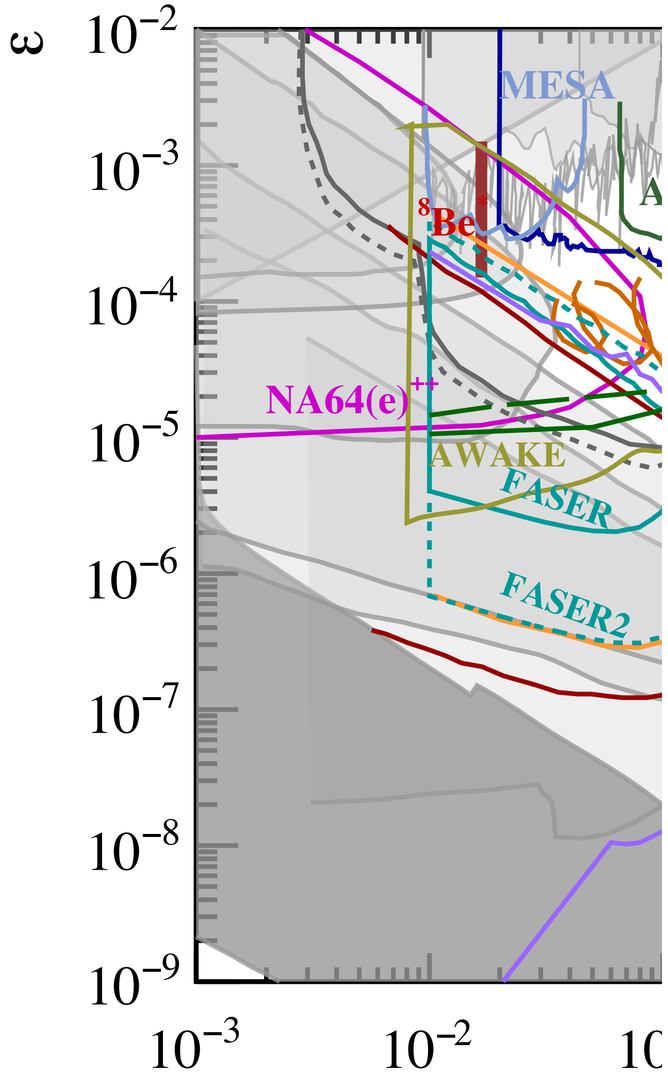

- NA62 in dump mode
- dark photon searches at MESA
- FASER
- FASER2 (future prospect)

[2005.01515]

Almost excluded for $m'_A < 0.1\,\mathrm{GeV}$

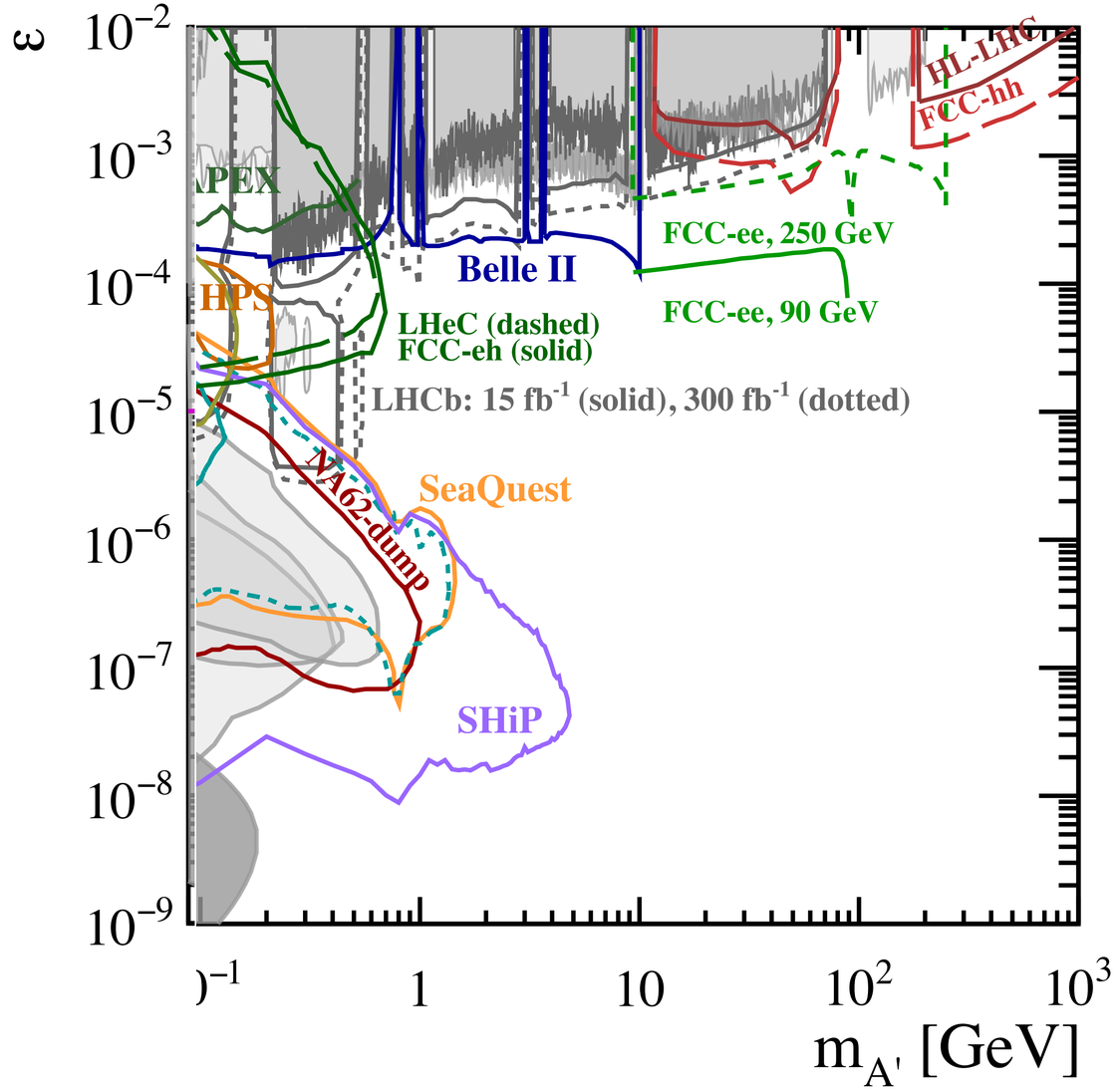

- Belle II
- LHCb
- SHIP
- Weaker constraints for heavier dark photon

[2005.01515]

How about a heavy dark Z with a mass above 1 TeV?

Bounds are weak at pp colliders

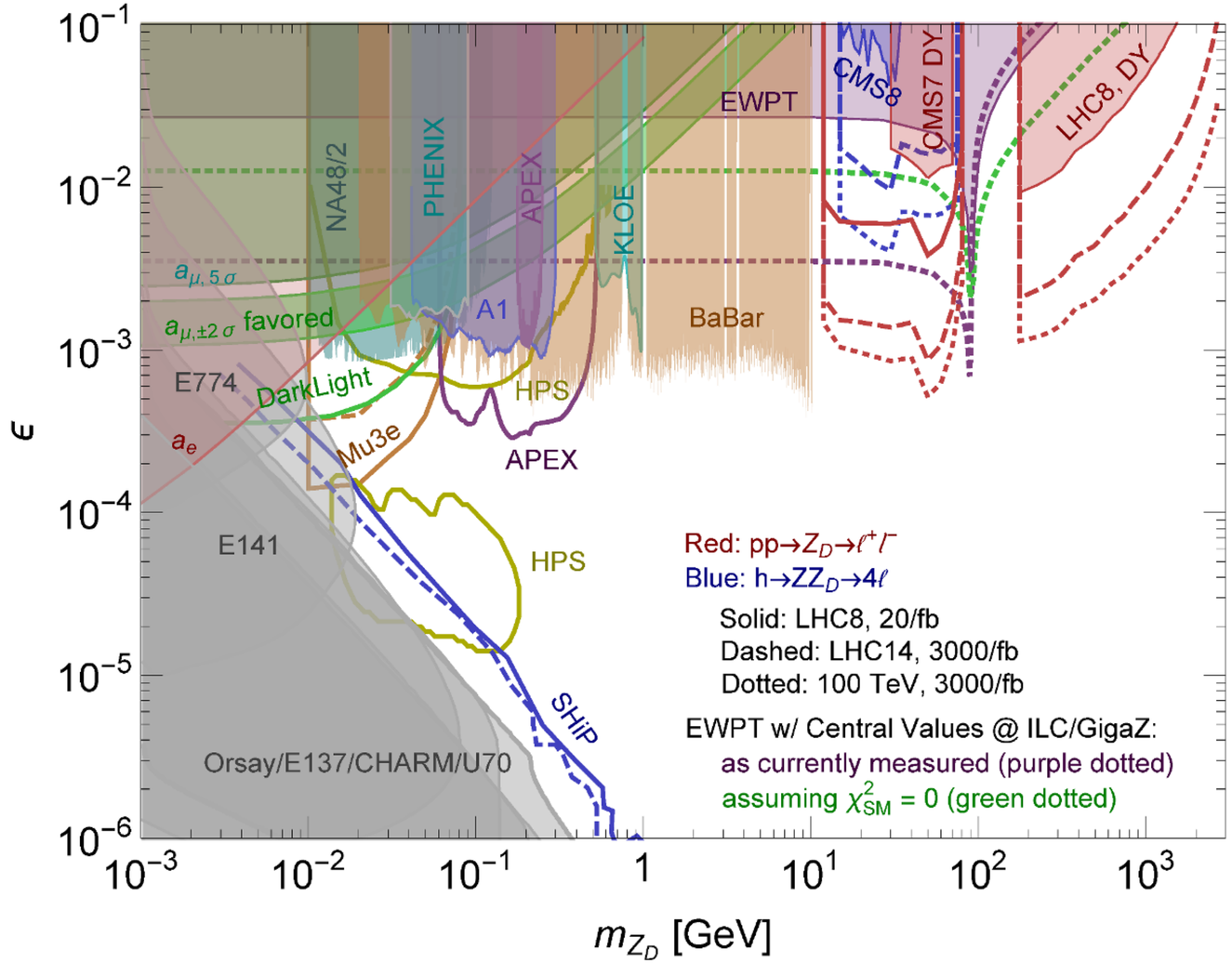

[1412.0018]

Bounds are weak at pp colliders

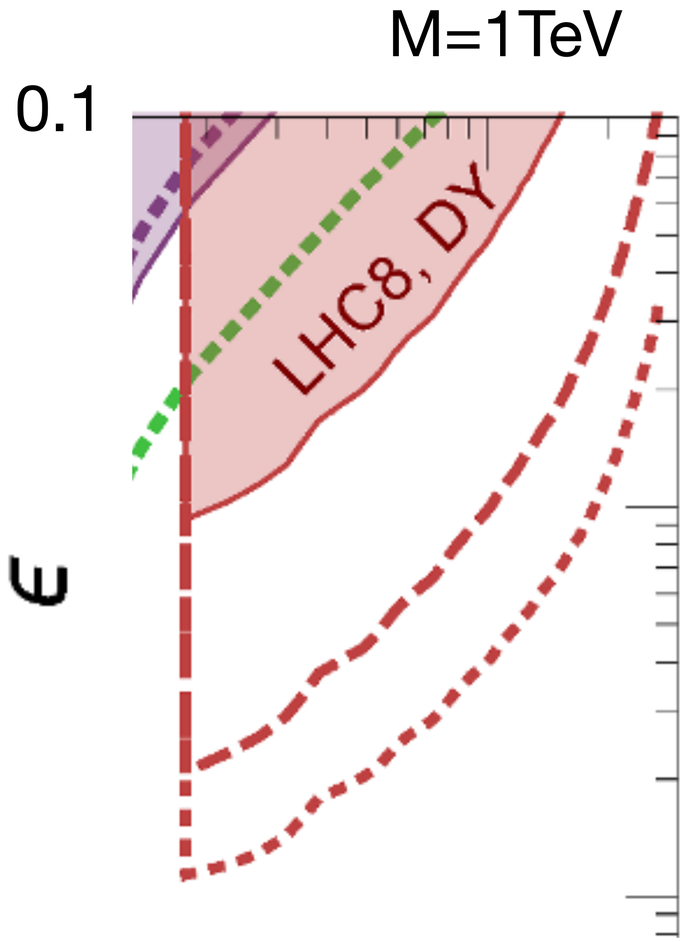

- Solid: LHC8 w/ 20/fb
- Dashed: LHC14 w/3/ab
- Dotted: 100 TeV pp w/3/ab
- ε sensitivity becomes drastically weaker as the dark Z is heavier.
- Why?

[2005.01515]

Inability of a pp collider to use the full collision energy

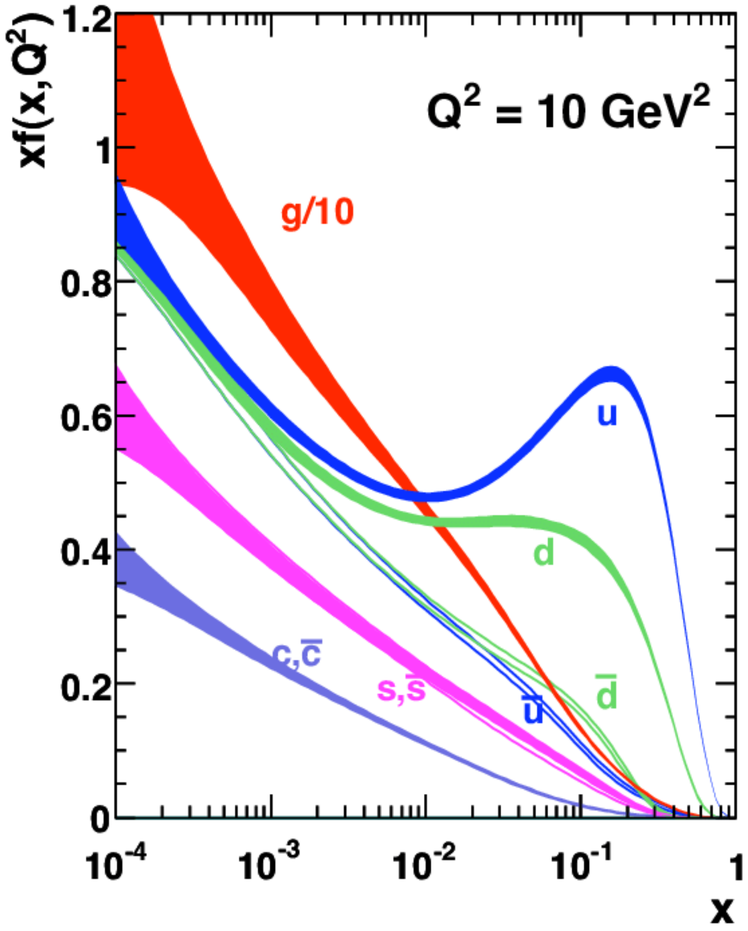

- At 100 TeV pp collider,
- $\sigma(pp \to Z_D)/\varepsilon^2 = 140\,\text{pb}$ for $M_{Z'} = 1$ TeV
- $\sigma(pp \to Z_D)/\varepsilon^2 = 0.5\,\text{pb}$ for $M_{Z'} = 5$ TeV
- $\sigma(pp \to Z_D)/\varepsilon^2 = 0.03\,\text{pb}$ for $M_{Z'} = 10$ TeV

Let's win this race:

Z_D decays into the SM particles

III. Multi-TeV Muon Collider

Muon

- Half-life 2.2 μs
- Mass 105.658 MeV/c
- 207 times electron mass

Why muon?

1. Once accelerated: $E \sim 1$ TeV, $\gamma \sim 10^4$, $c\gamma\tau \simeq 6{,}600$ km
2. Much less synchrotron radiation energy loss than electrons:
3. Compact

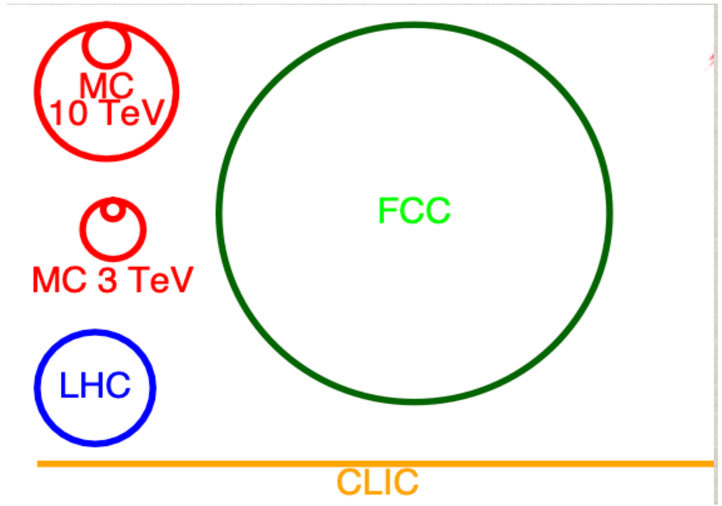

4. Luminosity scales with c.m. energy $\mathscr{L} \propto E^2_{\text{c.m.}}$: high c,m, energy
5. Smaller beam-energy spread: $\Delta E/E \sim 0.1\,\%$

Challenges

(1) Neutrino beams from the muon decay

(2) Beam induced background

(3) Shielding the Detector from BIBs

(4) Muon production

(1) Neutrino beams 1

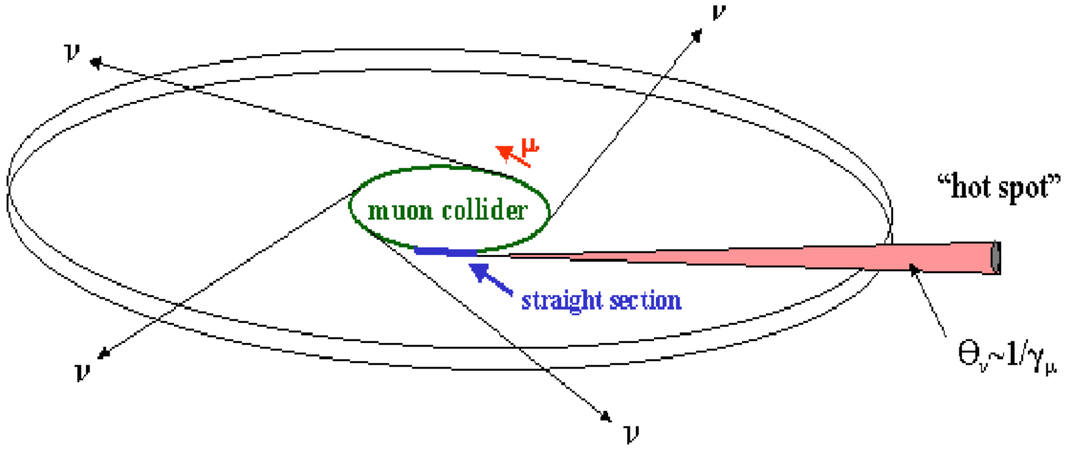

- Muon decay: $\mu \rightarrow e\nu_e\nu_\mu$ with almost 100% BR.
- Neutrino beam opening angle θ_ν about the central axis of the beam is proportional to 1/γ. So, θ_ν is very small.
- The neutrinos are almost aligned with the muon beam direction, resulting in a disk of neutrino radiation.

(1) Neutrino beams 2: Hot spot

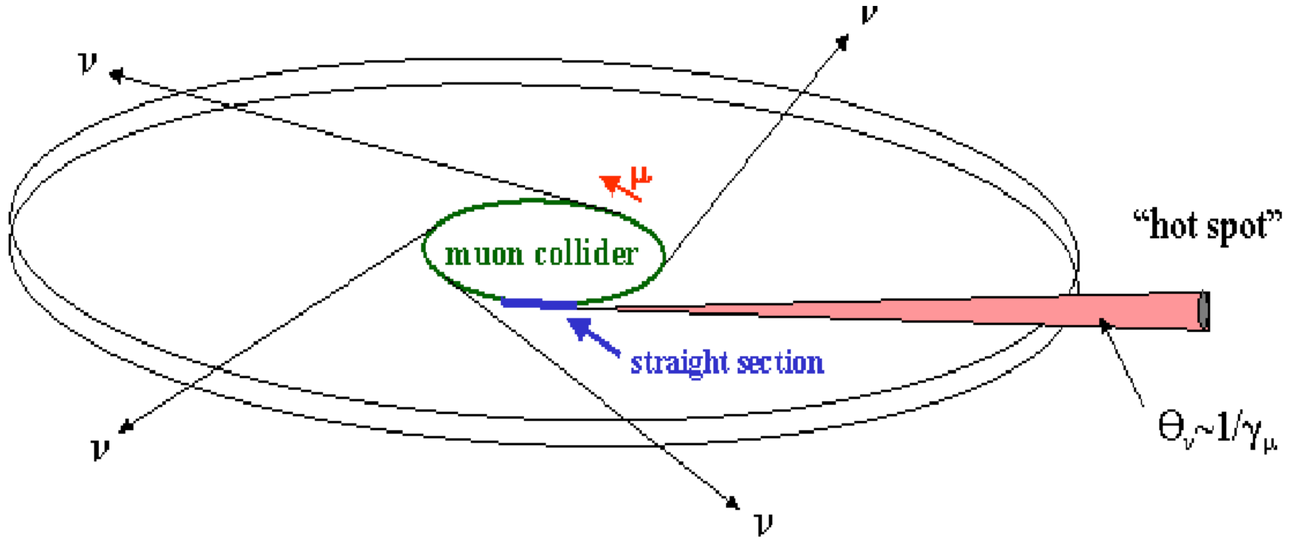

- A collider ring consists of curved sections and straight sections.
- When muons decay in the straight sections, the neutrinos continue traveling in the same direction. We have radiation hot spots.
- Multi-TeV neutrinos can interact with matter and produce showers of secondary particles, including neutrons.
- We need to guarantee the safety and legal limits.

(2) Beam Induced Backgrounds (BIB)

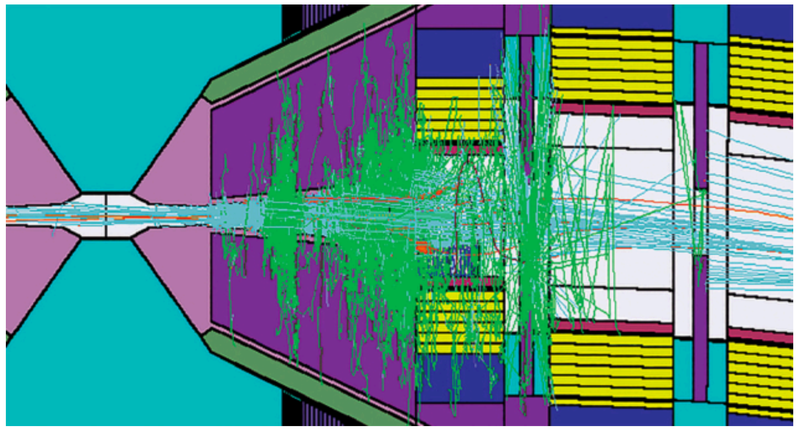

- The muon decays generates electrons or positrons.
- They can interact with the collider's structure and other materials.
- Additional secondary particles like photons, neutrons, and other radiation forms.
- Without proper shielding, the detectors would be harmed.

(3) Shielding the detector from BIB

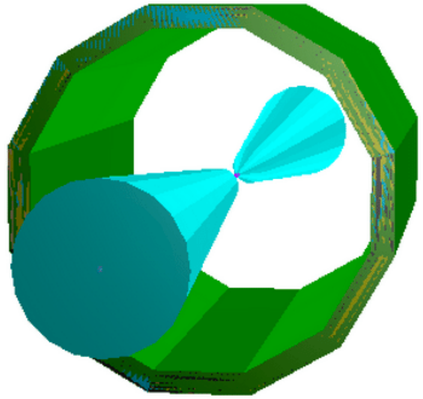

Tungsten nozzle

- Tungsten is a dense, hard metal with a high melting point.
- There is a rapidity limitation such that $|\eta| < 2.5$

(4) Muon Production

- Usual Muon Source
  - Colliding protons with a target material.
  - Many pions decay into muons and neutrinos.
  - The produced muons have a wide range of energies and directions.

Muon Beam Cooling

- Why?
  - Muons produced in proton collisions have a wide range of energies and directions. **High emittance.**
  - Need to "cool" the muon beam, i.e., reducing the spread in position and momentum of the muons. Low emittance.
- Three Cooling Methods
  1. Ionization Cooling
  2. LEMMA
  3. Tristan

1. Ionization Muon Beam Cooling

- Passing muons through an energy absorbing material (the absorber) where the particles loose both longitudinal and transverse momentum.
- A set of radio frequency cavities restore the lost longitudinal momentum.
- The net result is to reduce transverse momentum. The beam is “cooled”.

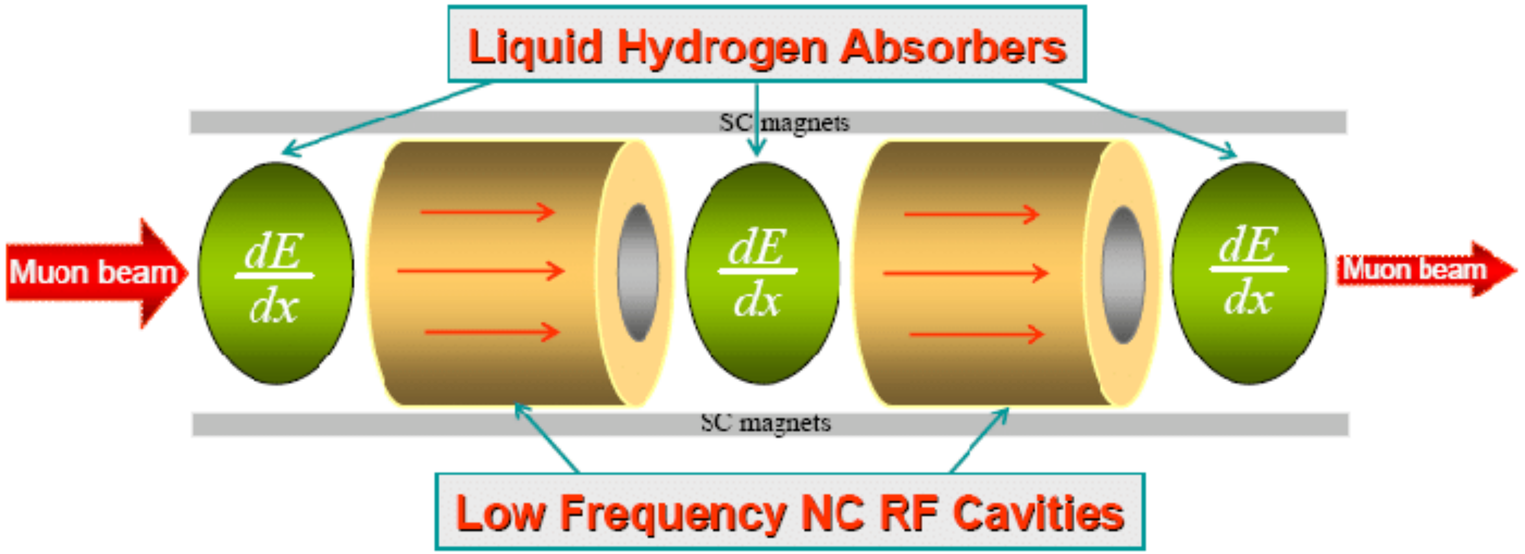

Transverse ionization cooling achieved by MICE

Article

Demonstration of cooling by the Muon Ionization Cooling Experiment

https://doi.org/10.1038/s41586-020-1958-9

MICE collaboration*

Received: 22 July 2019

MICE stands for Muon Ionization Cooling Experiment.

2. LEMMA

LEMMA

(Low EMittance Muon Accelerator)

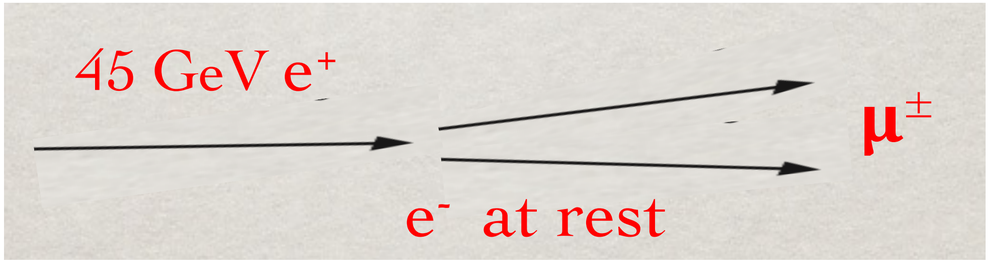

J.P. Delahauge et al., arXiv:1901.06150

- From direct μ pair production:
- Muons produced from $e^+e^- \rightarrow \mu^+\mu^-$ at the $\mu^+\mu^-$ threshold ($\sqrt{s} \simeq 0.212$ GeV) in asymmetric collisions (to collect $\mu^+\mu^-$)
- A major advantage of this proposal is the lack of cooling of the muons Ionization Cooling:

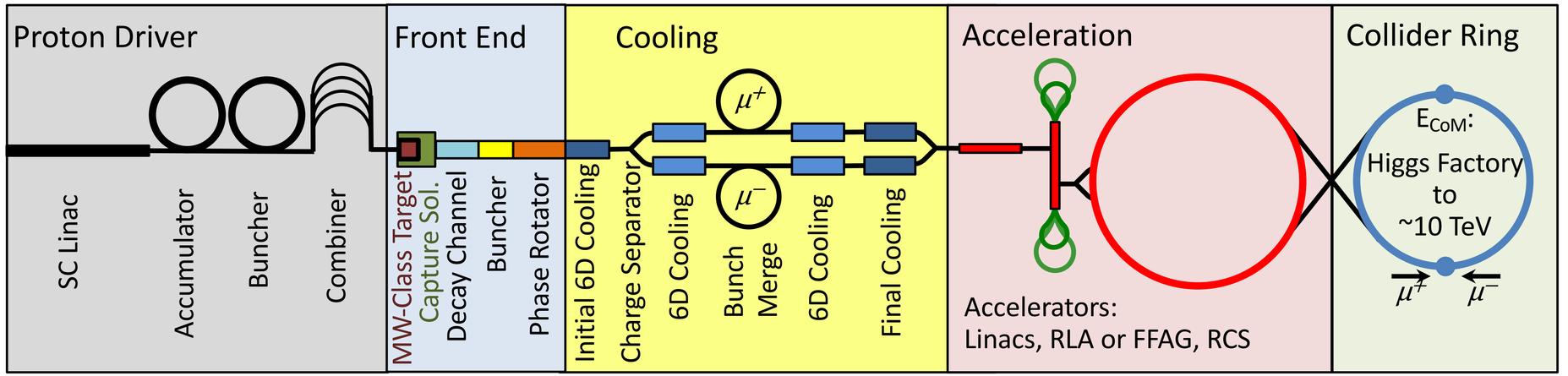

Low EMmittance Muon Accelerator (LEMMA): 10^{11} μ pairs/sec from e^+e^- interactions. The small production emittance allows lower overall charge in the collider rings – hence, lower backgrounds in a collider detector and a higher potential CoM energy due to neutrino radiation.

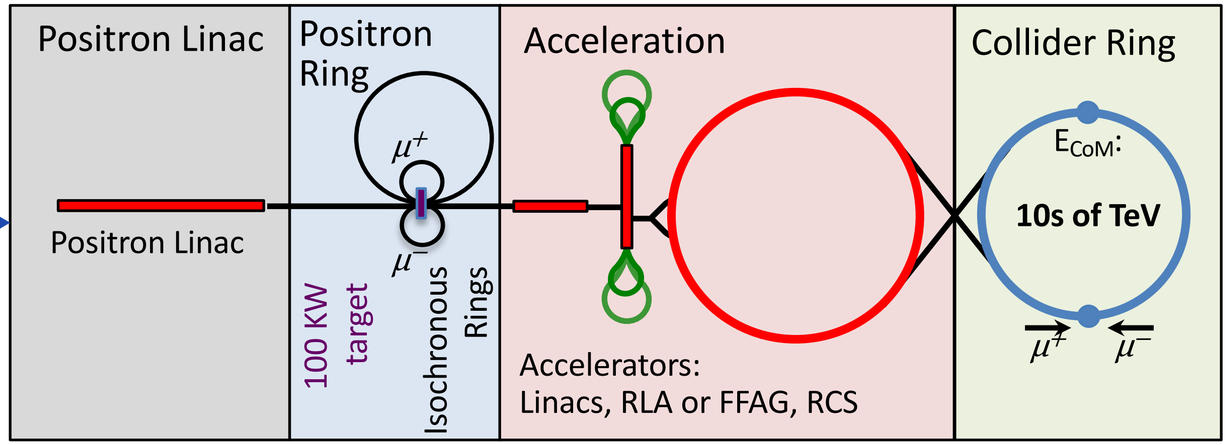

Ref. M. Boscolo et al., "*The future prospects of muon colliders and neutrino factories*", RAST 10 (2019) 189-214 ArXiv.1808.01858

No cooling for LEMMA

3. μTRISTAN

PTEP

Prog. Theor. Exp. Phys. **2022** 053B02(16 pages)
DOI: 10.1093/ptep/ptac059

μTRISTAN

Yu Hamada[1], Ryuichiro Kitano[1,2], Ryutaro Matsudo[1], Hiromasa Takaura[1,*], and Mitsuhiro Yoshida[2,3]

[1]*KEK Theory Center, Tsukuba 305-0801, Japan*
[2]*Graduate University for Advanced Studies (Sokendai), Tsukuba 305-0801, Japan*
[3]*KEK Accelerator Department, Tsukuba 305-0801, Japan*
*E-mail: takaura.phys@gmail.com

Received January 21, 2022; Revised March 18, 2022; Accepted March 28, 2022; Published March 30, 2022

- The ultra-cold muon technology developed for the muon g – 2 experiment at J-PARC
- There is a possibility of new collider experiments by accelerating the μ^+ beam up to 1 TeV.

3. μTRISTAN: Conceptual design of the μ+e–/μ+μ+ collider.

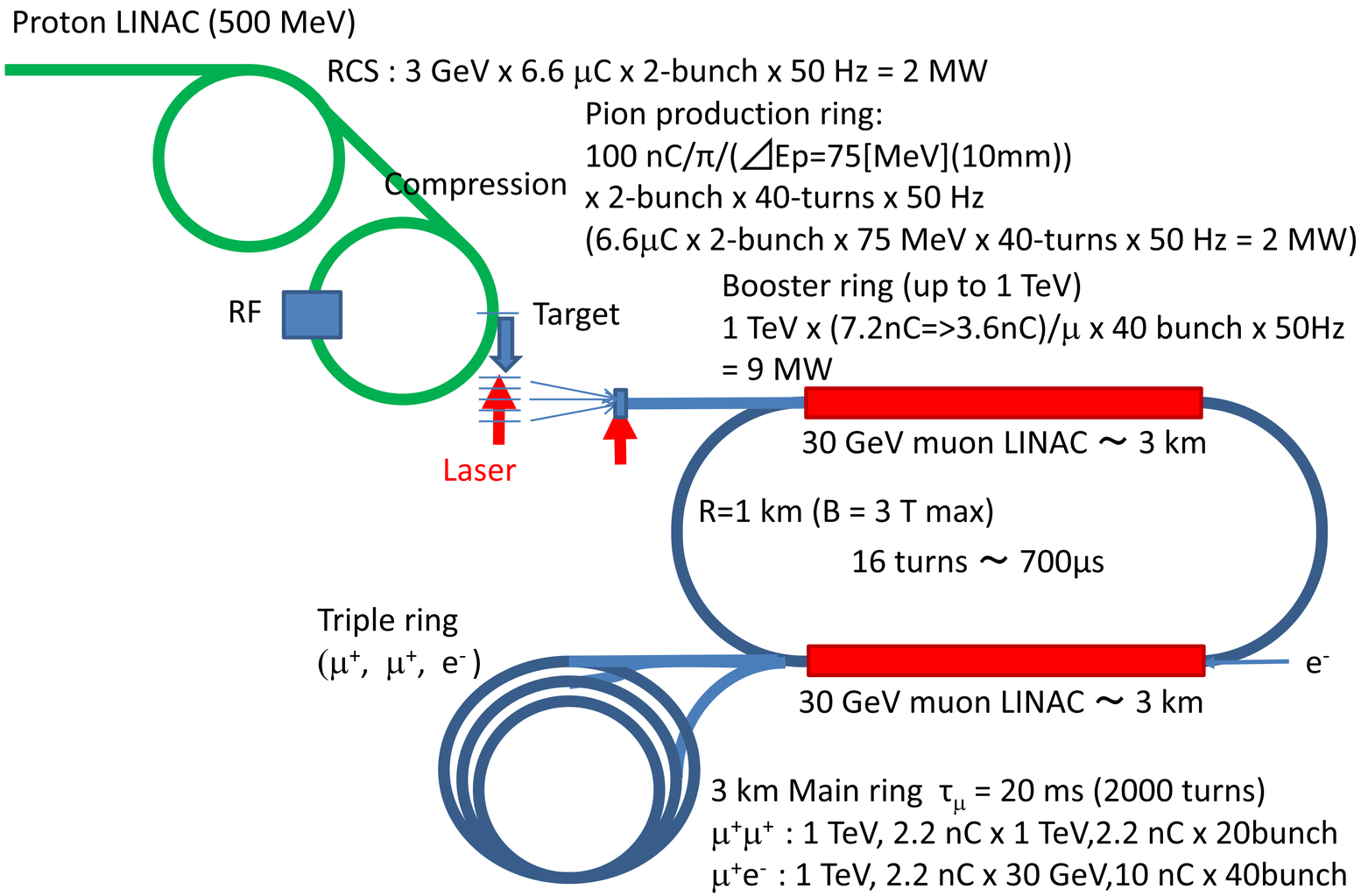

Fig. 1. Conceptual design of the $\mu^+e^-/\mu^+\mu^+$ collider.

3. μTRISTAN: Conceptual design of the μ+e–/μ+μ+ collider.

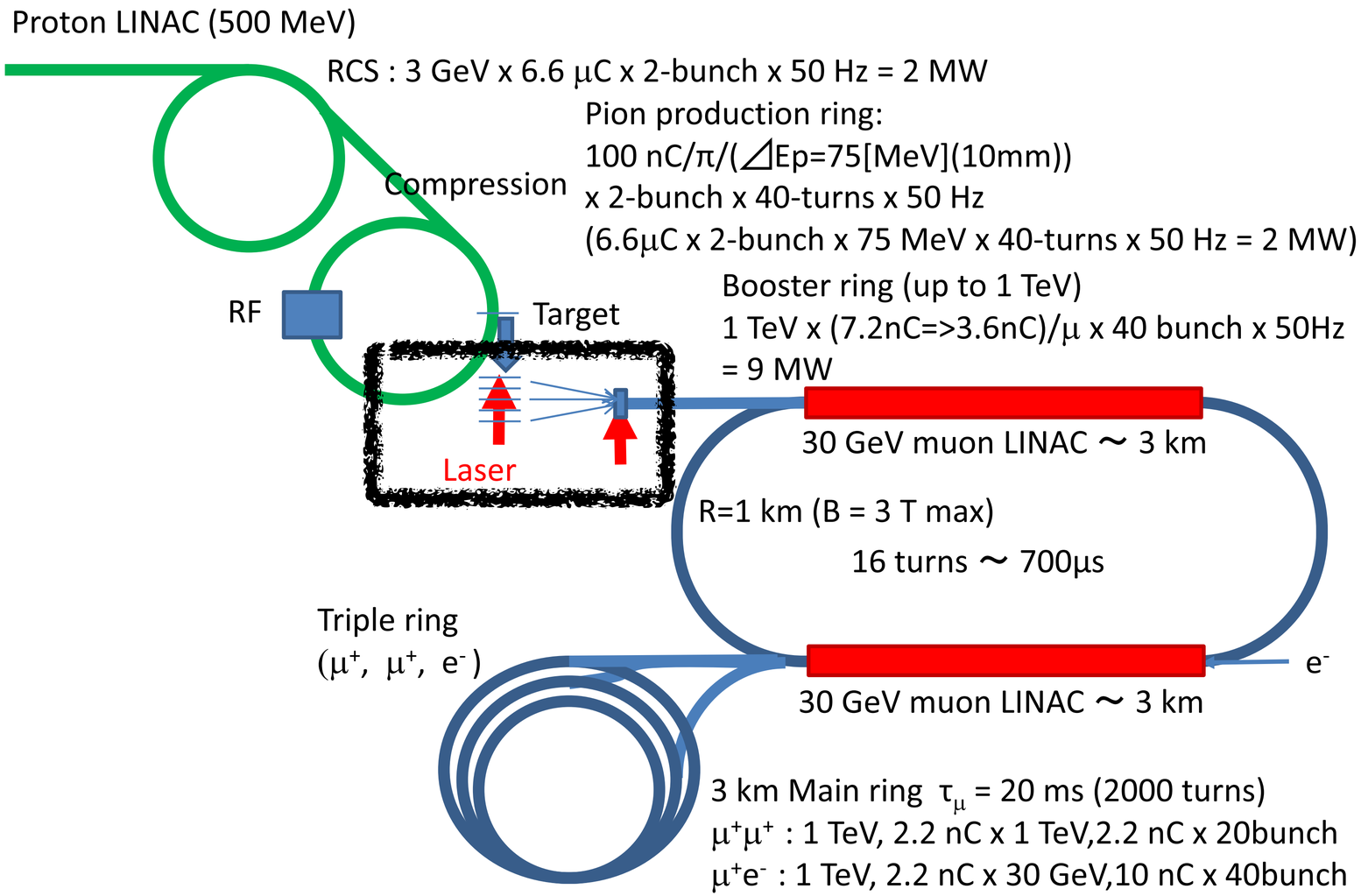

Fig. 1. Conceptual design of the $\mu^+e^-/\mu^+\mu^+$ collider.

2. μTRISTAN: Ultra-cold muons and μ+ accelerator

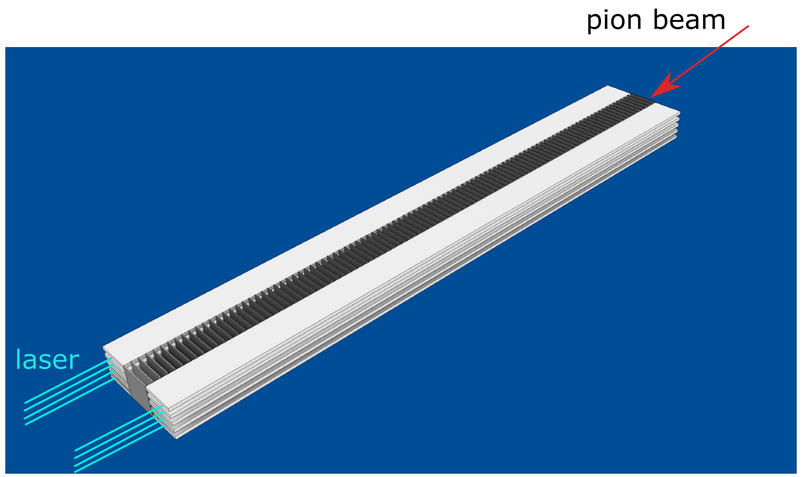

- Deliver an intense proton beam with 3 GeV to the pion production target.
- The cross section of $p + C \rightarrow \pi^+ + X$ is 150 mb
- The π^+'s are transported to the multi-layer pion stopping target (tungsten foil), producing μ^+.
- μ^+ are transported to the multiple-layered silica aerogel target, forming the $\mu^+ e^-$ bound state.

2. μTRISTAN: Ultra-cold muons and μ+ accelerator

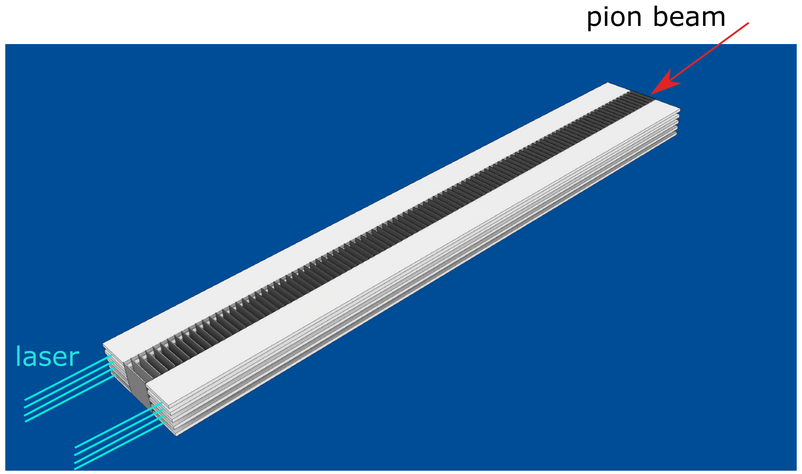

- Thermal diffusion of the μ^+e^- bound state with the aerogel at a low temperature.
- μ^+e^- have a low thermal energy and, consequently, a low velocity spread.
- Shoot a Lyman-α laser, which removes the electron (ionized muon).
- But no additional kinetic energy to the remaining muon.
- The muons retain the small velocity.
- Then reaccelerate the muons so that they have a very small momentum spread.

3. μTRISTAN: Conceptual design of the μ+e–/μ+μ+ collider.

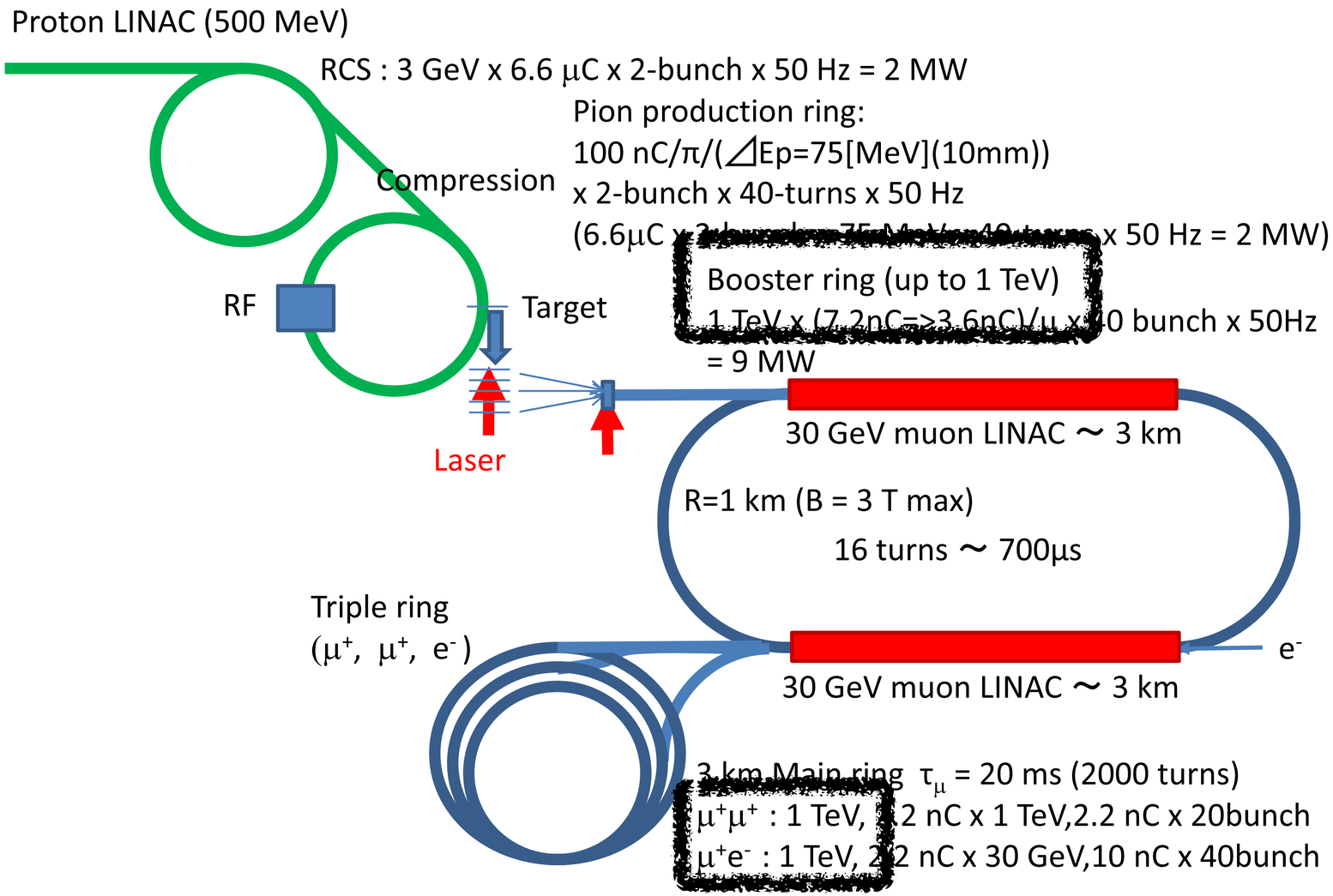

Fig. 1. Conceptual design of the $\mu^+e^-/\mu^+\mu^+$ collider.

IV. Dark Z at the MuC

Model setup

A. Lagrangian:

$$\mathscr{L} \supset -\frac{1}{4}\,\tilde{B}_{\mu\nu}\,\tilde{B}^{\mu\nu} - \frac{1}{4}\,\tilde{Z}_{\mathrm{D}\mu\nu}\,\tilde{Z}_{\mathrm{D}}^{\mu\nu} - \frac{1}{2}\,\frac{\varepsilon}{c_{\mathrm{W}}}\,\tilde{Z}_{\mathrm{D}\mu\nu}\,\tilde{B}^{\mu\nu} + \frac{1}{2}\,M_{D,0}^{2}\,\tilde{Z}_{\mathrm{D}}^{\mu}\,\tilde{Z}_{\mathrm{D}\mu}\,,$$

B. Our focus:

$$M_{Z_{\mathrm{D}}} \in [1, 10]\ \mathrm{TeV}, \quad \varepsilon < 10^{-1}.$$

$$\boxed{\delta_m = \frac{m_{Z,0}}{M_{D,0}} \ll 1,}$$

C. The mass eigenstates:

$$\begin{pmatrix} Z \\ Z_{\mathrm{D}} \end{pmatrix} = \begin{pmatrix} c_\alpha & s_\alpha \\ -s_\alpha & c_\alpha \end{pmatrix} \begin{pmatrix} Z_0 \\ Z_{\mathrm{D},0} \end{pmatrix}$$

$$\boxed{\alpha = -t_{\mathrm{W}}\delta_m^2\varepsilon + \mathcal{O}\left(\delta_m^4\varepsilon\right)}$$

Different interactions between Z and Z’

A. Interaction Lagrangian:

$$-\mathscr{L}_{\rm int} = \frac{g}{c_{\rm W}}\,\hat{g}_Z^f Z^\mu \bar{f}\gamma_\mu f + \varepsilon\,\frac{g}{c_{\rm W}}\,\hat{g}_{Z_{\rm D}}^f Z_{\rm D}^\mu \bar{f}\gamma_\mu f.$$

B. The normalized couplings

$$\hat{g}_Z^f = T_{3f} - Q_f s_{\rm W}^2 - (T_{3f} - Q_f) t_{\rm W}^2 \delta_m^2 \varepsilon^2 + \mathcal{O}(\delta_m^4 \varepsilon^2),$$
$$\hat{g}_{Z_{\rm D}}^f = (T_{3f} - Q_f) t_{\rm W} + \mathcal{O}(\delta_m^2),$$

$$\frac{\hat{g}_{Z_{\rm D}}^{\nu_L}}{\hat{g}_Z^{\nu_L}} = t_{\rm W} \approx 0.548,$$
$$\frac{\hat{g}_{Z_{\rm D}}^{e_R}}{\hat{g}_Z^{e_R}} = \frac{1}{s_{\rm W} c_{\rm W}} \approx 2.37,$$

C. Enhanced branching ratios into an electron pair.

Branching Ratios of the heavy dark Z

$$\mathrm{Br}(Z_\mathrm{D} \to q\bar{q}) \approx 0.40,$$
$$\mathrm{Br}(Z_\mathrm{D} \to e^+e^-) \approx 0.12,$$
$$\mathrm{Br}(Z_\mathrm{D} \to \nu\bar{\nu}) \approx 0.074,$$
$$\mathrm{Br}(Z_\mathrm{D} \to t\bar{t}) \approx 0.13,$$
$$\mathrm{Br}(Z_\mathrm{D} \to W^+W^-) \approx 0.019,$$
$$\mathrm{Br}(Z_\mathrm{D} \to ZH) \approx 0.013,$$

Branching Ratios of the heavy dark Z

$$\mathrm{Br}(Z_\mathrm{D} \to q\bar{q}) \approx 0.40,$$

$$\mathrm{Br}(Z_\mathrm{D} \to e^+e^-) \approx 0.12,$$

$$\mathrm{Br}(Z_\mathrm{D} \to \nu\bar{\nu}) \approx 0.074,$$

$$\mathrm{Br}(Z_\mathrm{D} \to t\bar{t}) \approx 0.13,$$

$$\mathrm{Br}(Z_\mathrm{D} \to W^+W^-) \approx 0.019,$$

$$\mathrm{Br}(Z_\mathrm{D} \to ZH) \approx 0.013,$$

Suppressed!

Branching Ratios of the heavy dark Z

$$\mathrm{Br}(Z_\mathrm{D} \to q\bar{q}) \approx 0.40,$$

$$\mathrm{Br}(Z_\mathrm{D} \to e^+e^-) \approx 0.12,$$

$$\mathrm{Br}(Z_\mathrm{D} \to \nu\bar{\nu}) \approx 0.074,$$

$$\mathrm{Br}(Z_\mathrm{D} \to t\bar{t}) \approx 0.13,$$

$$\mathrm{Br}(Z_\mathrm{D} \to W^+W^-) \approx 0.019,$$

$$\mathrm{Br}(Z_\mathrm{D} \to ZH) \approx 0.013,$$

Enhanced!

Let's win this race!

Retain as much signal events as possible!

$$Z_{\rm D} \to jj + X, \quad Z_{\rm D} \to e^+e^-.$$

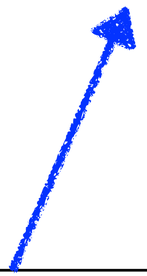

$q\bar{q}$, $\tau^+\tau^-$, $t\bar{t}$, and W^+W^-.

Production Channels at the MuC

$$\mu^+\mu^- \to Z_{\mathrm{D}}\gamma,$$
$$\mu^+\mu^- \to Z_{\mathrm{D}}\nu\bar{\nu},$$
$$\mu^+\mu^- \to Z_{\mathrm{D}}\mu^+\mu^-$$

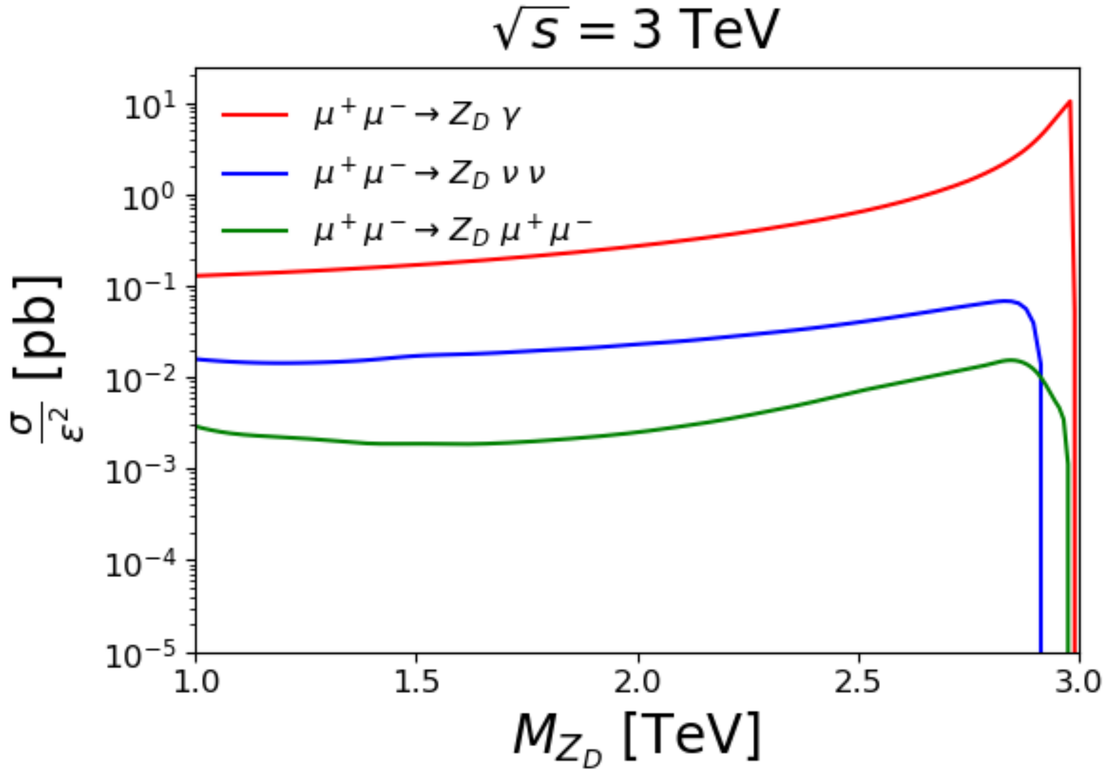

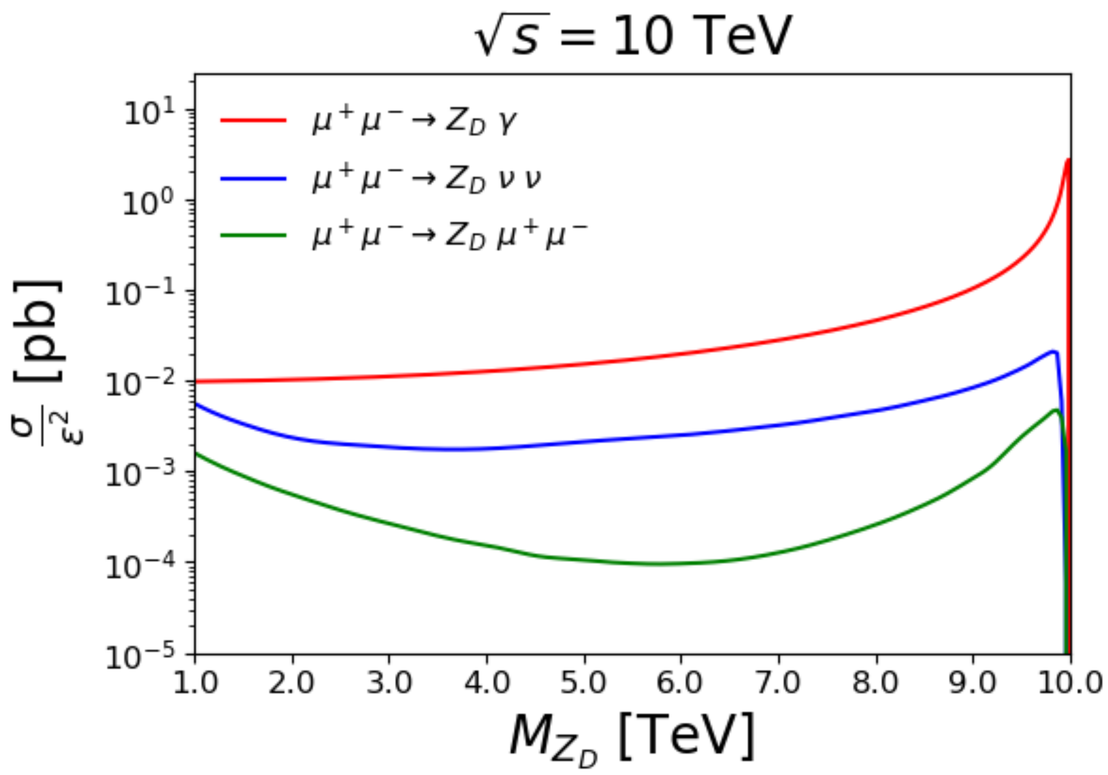

Production Channels at the MuC

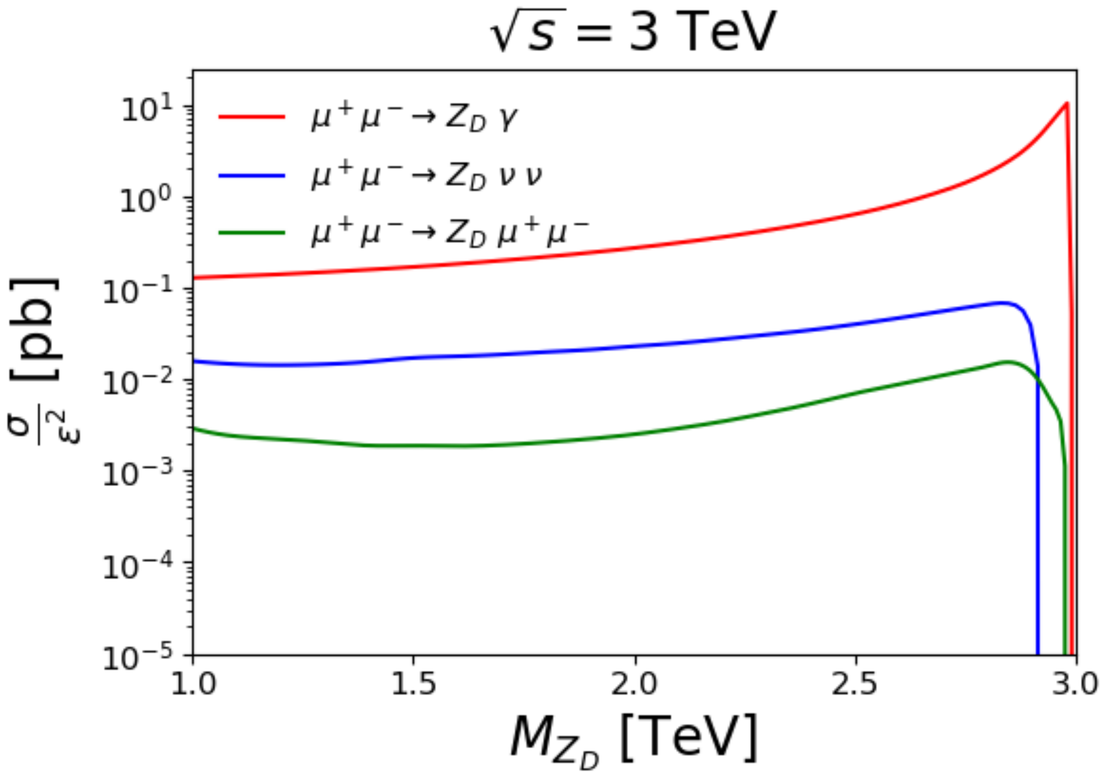

- $Z_D\gamma$ has the largest cross section.
- $\sigma(\mu\mu \to Z_D\gamma)/\varepsilon^2$ increases as M_{Z_D} increases.
- As M_{Z_D} approaches $\sqrt{s}$, $\sigma(\mu\mu \to Z_D\gamma)/\varepsilon^2$ sharply increases since the associated soft photon makes the process effectively $2 \to 1$.

Production Channels at the MuC

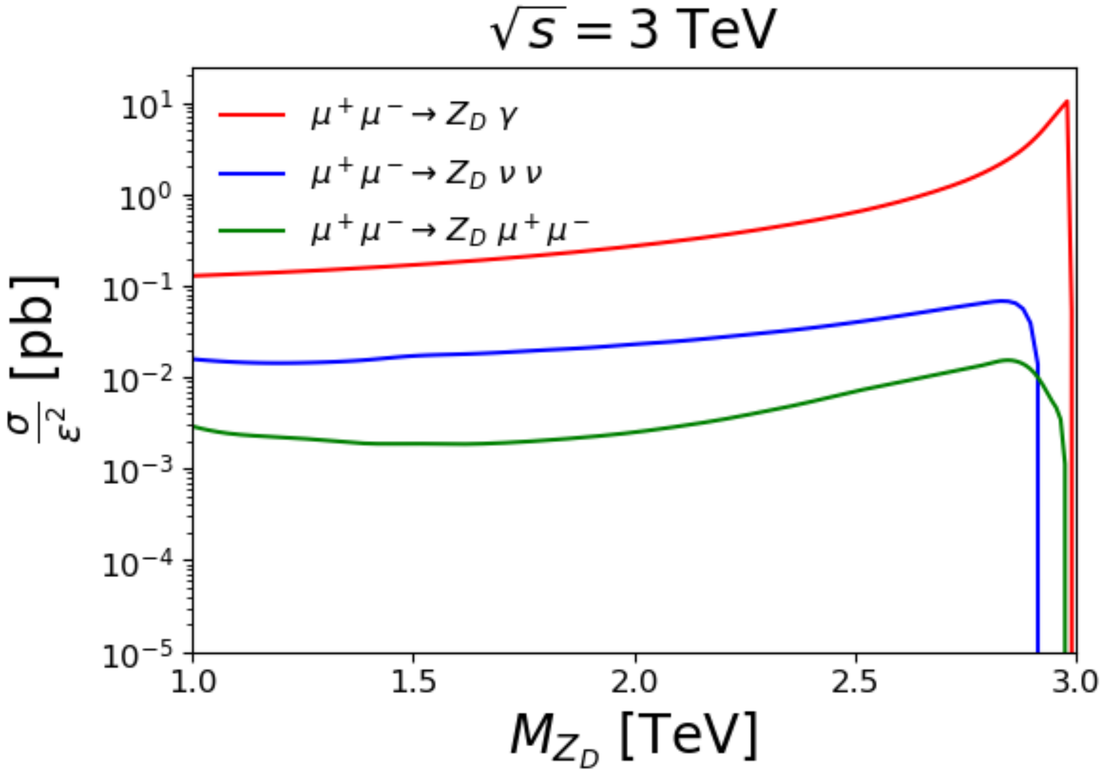

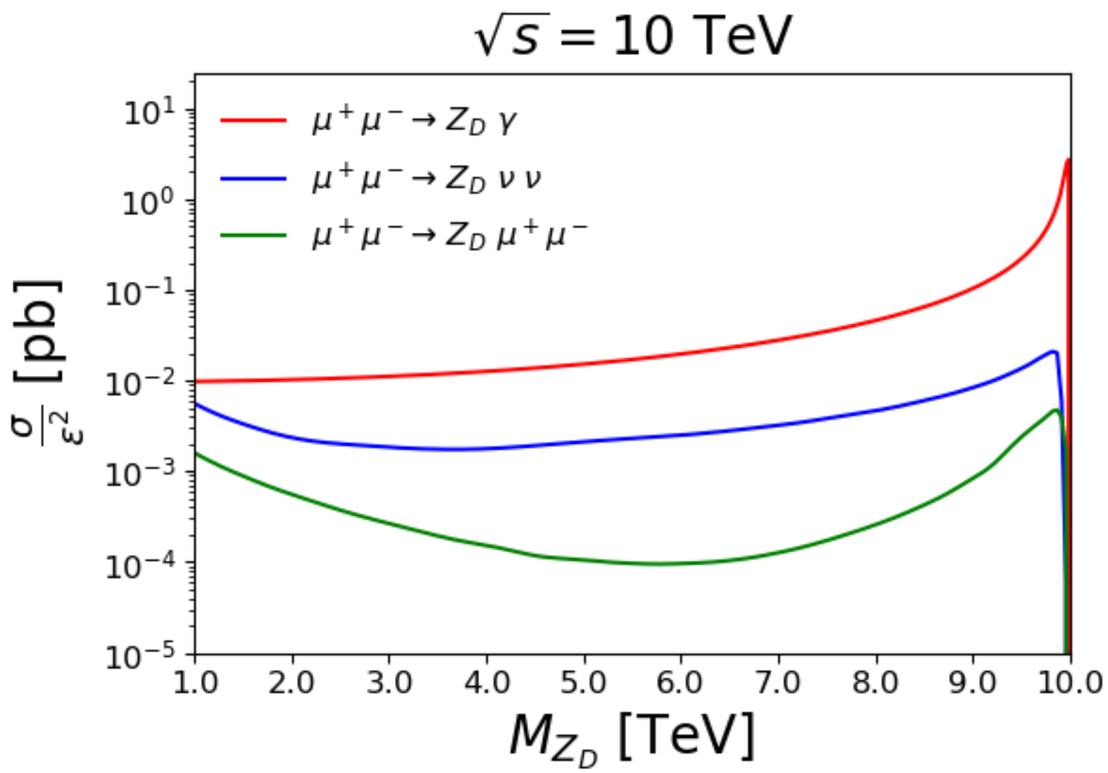

$\sigma(\mu\mu \to Z_D\gamma)/\varepsilon^2$ is larger at the 3 TeV MuC.

Focus on the production of

$$\mu^+\mu^- \to Z_D\gamma$$

Precision Measurement of M_{Z_D} at Muon Colliders

- Invariant mass peak can be measured in the $Z_D \to e^+e^-$ mode, i.e., m_{ee}

Precision Measurement of M_{Z_D} at Muon Colliders

- Invariant mass peak can be measured in the $Z_D \to e^+e^-$ mode, i.e., m_{ee}
- For $Z_D \to jjX$, the invariant mass does not correspond to M_{Z_D}

Precision Measurement of M_{Z_D} at Muon Colliders

- Invariant mass peak can be measured in the $Z_D \to e^+e^-$ mode, i.e., m_{ee}
- For $Z_D \to jjX$, the invariant mass does not correspond to M_{Z_D}
- At the MuC, the recoil mass of the photon matches M_{Z_D}.

$$\boxed{m^2_{\text{recoil}} = s - 2\sqrt{s}E_\gamma = M^2_{Z_\text{D}}.}$$

Precision Measurement of M_{Z_D} at Muon Colliders

- Invariant mass peak can be measured in the $Z_D \to e^+e^-$ mode, i.e., m_{ee}
- For $Z_D \to jjX$, the invariant mass does not correspond to M_{Z_D}
- At the MuC, the recoil mass of the photon matches M_{Z_D}.

$$\boxed{m^2_{\rm recoil} = s - 2\sqrt{s}E_\gamma = M^2_{Z_{\rm D}}.}$$

- Usually, a universal cut is adopted!

$$|m_{{\rm recoil},ee} - M_{Z_{\rm D}}| < 10 \ {\rm GeV}$$

Photon/electron energy resolution

- The recoil was distribution is sensitive to the photon energy resolution at the detector.

$$\frac{\Delta E_\gamma}{E_\gamma} = \frac{a}{\sqrt{E_\gamma}} \oplus b \oplus \frac{c}{E_\gamma},$$

D

Photon/electron energy resolution

- The recoil was distribution is sensitive to the photon energy resolution at the detector.

$$\frac{\Delta E_\gamma}{E_\gamma} = \frac{a}{\sqrt{E_\gamma}} \oplus b \oplus \frac{c}{E_\gamma},$$

- The higher E_γ, the larger ΔE_γ, the wider the recoil mass peak ➡ Heavy M_{Z_D}

- Similarly, the higher E_e, the larger ΔE_e, the wider the m_{ee} peak ➡ Light M_{Z_D}

Detector-level simulation

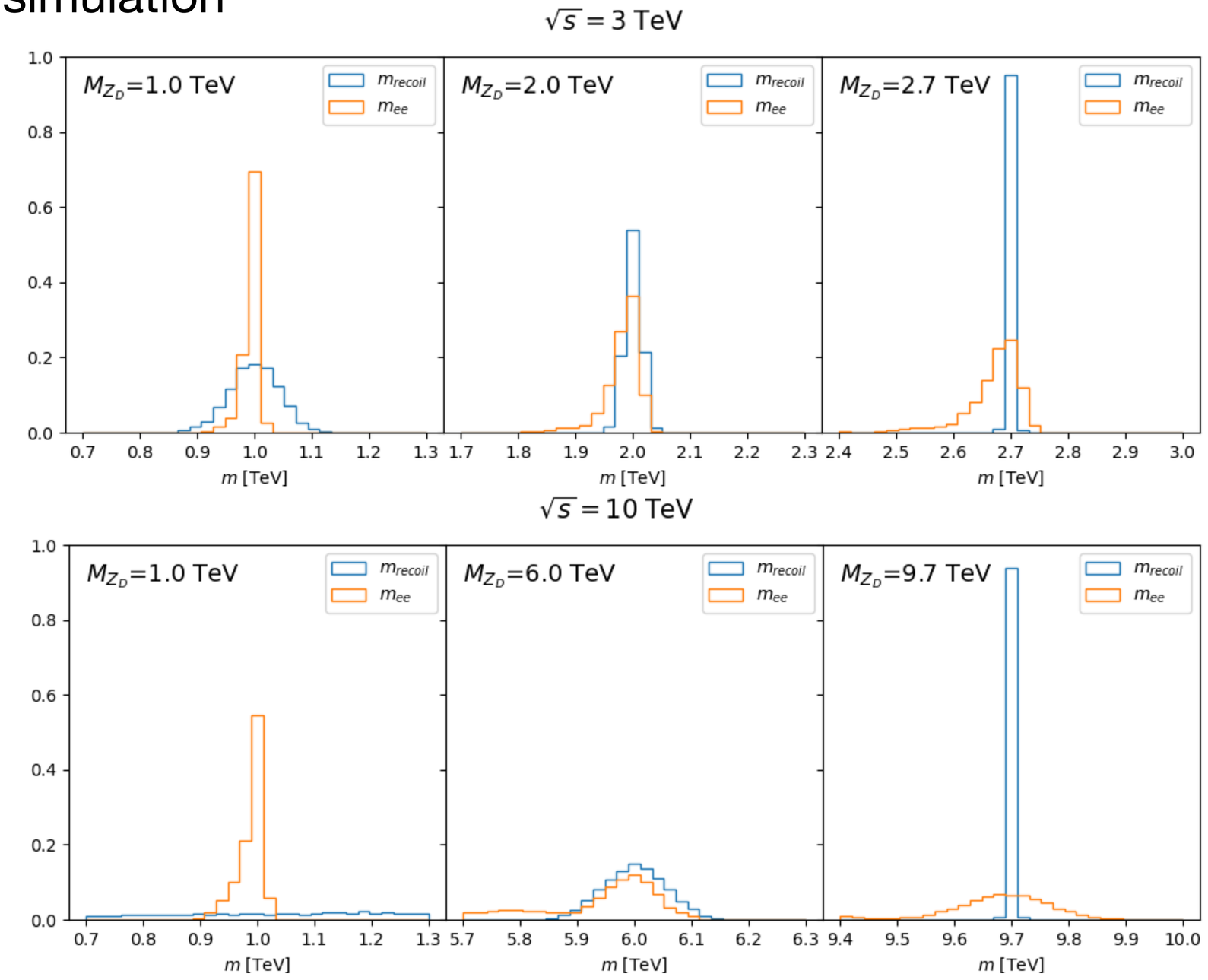

Goal: Find optimal mass windows for M_{Z_D} at a given $\sqrt{s}$

- Using multiple benchmark points for different M_{Z_D}, we fit the detector-level simulation results with a Gaussian function.
- The standard deviation of this fitted Gaussian was then assigned as the mass windows:

$$|m_{\text{recoil}} - M_{Z_{\text{D}}}| < 2\Delta m_{\text{recoil}}, \quad |m_{ee} - M_{Z_{\text{D}}}| < 2\Delta m_{ee}.$$

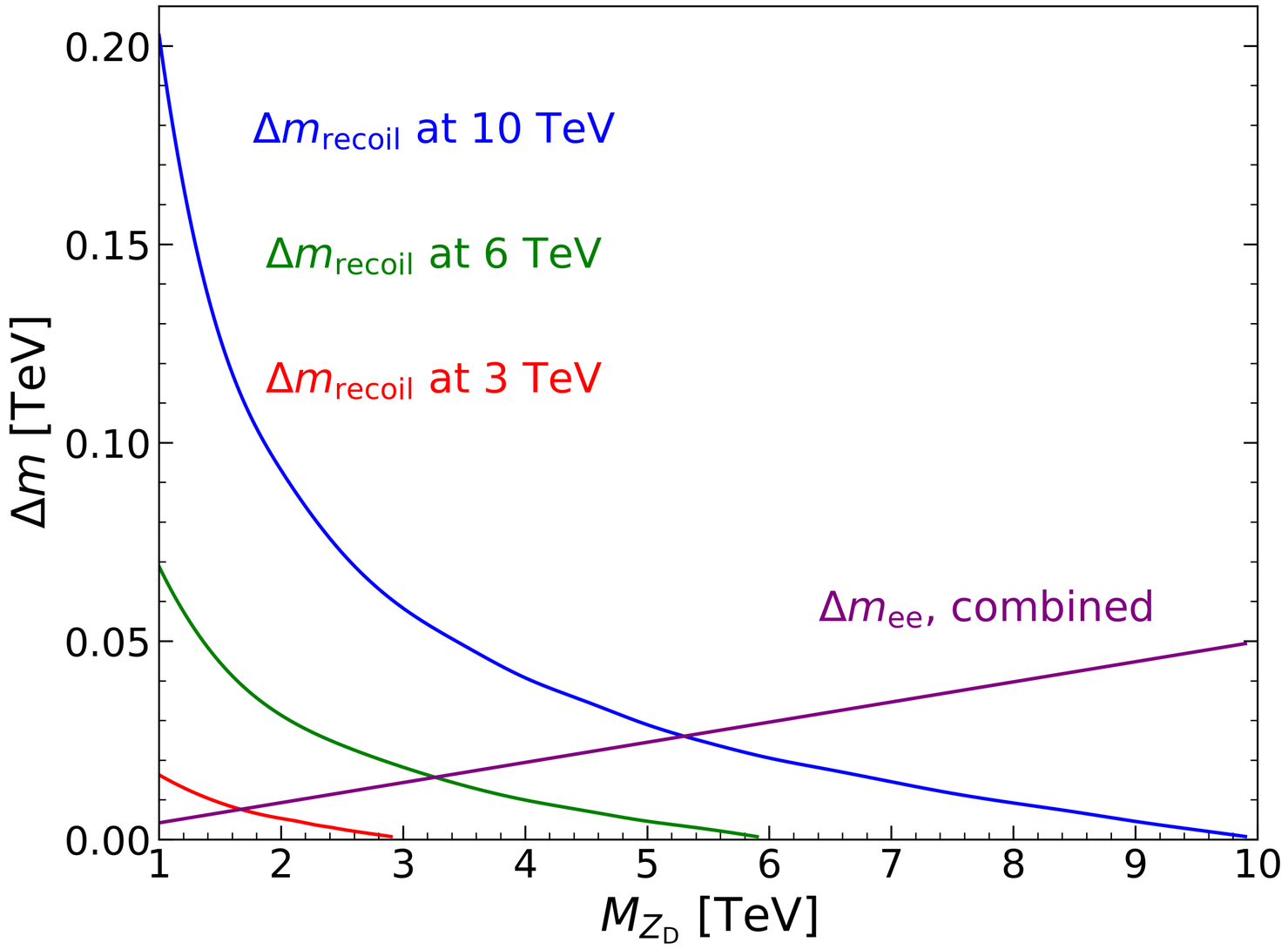

- Δm_{recoil} decreases with increasing M_{Z_D}.
- But Δm_{ee} increases with increasing M_{Z_D}.
- Δm_{recoil} increases with increasing $\sqrt{s}$.

V. Signal-to-Background analysis

Backgrounds

Background cross sections in units of fb			
Processes	$\sqrt{s} = 3$ TeV	$\sqrt{s} = 6$ TeV	$\sqrt{s} = 10$ TeV
$\mu^+\mu^- \to jj\gamma$	5.01×10	1.40×10	5.44
$\mu^+\mu^- \to e^+e^-\gamma$	9.31	2.75	1.10
$\mu^+\mu^- \to W^+W^-\gamma$	2.55×10	1.01×10	4.86
$\mu^+\mu^- \to \tau^+\tau^-\gamma$	5.37	1.63	6.67×10^{-1}
$\mu^+\mu^- \to t\bar{t}\gamma$	3.24	1.07	4.58×10^{-1}
$\mu^+\mu^- \to ZZ\gamma$	2.25	8.30×10^{-1}	3.82×10^{-1}

we imposed $p_T^{j_1,e_1} > 100$ GeV, $p_T^{j_2,e_2} > 20$ GeV, and $|\eta_{j,e}| < 2.5$.

Backgrounds

Background cross sections in units of fb			
Processes	$\sqrt{s} = 3$ TeV	$\sqrt{s} = 6$ TeV	$\sqrt{s} = 10$ TeV
$\mu^+\mu^- \to jj\gamma$	5.01×10	1.40×10	5.44
$\mu^+\mu^- \to e^+e^-\gamma$	9.31	2.75	1.10
$\mu^+\mu^- \to W^+W^-\gamma$	2.55×10	1.01×10	4.86
$\mu^+\mu^- \to \tau^+\tau^-\gamma$	5.37	1.63	6.67×10^{-1}
$\mu^+\mu^- \to t\bar{t}\gamma$	3.24	1.07	4.58×10^{-1}
$\mu^+\mu^- \to ZZ\gamma$	2.25	8.30×10^{-1}	3.82×10^{-1}

Dominant

we imposed $p_T^{j_1,e_1} > 100$ GeV, $p_T^{j_2,e_2} > 20$ GeV, and $|\eta_{j,e}| < 2.5$.

Backgrounds

Background cross sections in units of fb			
Processes	$\sqrt{s} = 3$ TeV	$\sqrt{s} = 6$ TeV	$\sqrt{s} = 10$ TeV
$\mu^+\mu^- \to jj\gamma$	5.01×10	1.40×10	5.44
$\mu^+\mu^- \to e^+e^-\gamma$	9.31	2.75	1.10
$\mu^+\mu^- \to W^+W^-\gamma$	2.55×10	1.01×10	4.86
$\mu^+\mu^- \to \tau^+\tau^-\gamma$	5.37	1.63	6.67×10^{-1}
$\mu^+\mu^- \to t\bar{t}\gamma$	3.24	1.07	4.58×10^{-1}
$\mu^+\mu^- \to ZZ\gamma$	2.25	8.30×10^{-1}	3.82×10^{-1}

Dominant

Sizable

we imposed $p_T^{j_1,e_1} > 100$ GeV, $p_T^{j_2,e_2} > 20$ GeV, and $|\eta_{j,e}| < 2.5$.

Inclusive Two-Jet Signal Analysis: Basic Selection

- $N_j \geq 2$ and $N_\gamma \geq 1$ with $|\eta_{j,\gamma}| < 2.5$;
- $p_T^{j_1} > 100$ GeV and $p_T^{j_2,\gamma} > 20$ GeV;
- Veto leptons, i.e., $N_e = N_\mu = 0$.

our dijet sample remains distinct from the e^+e^- mode

Inclusive Two-Jet Signal Analysis: Distributions

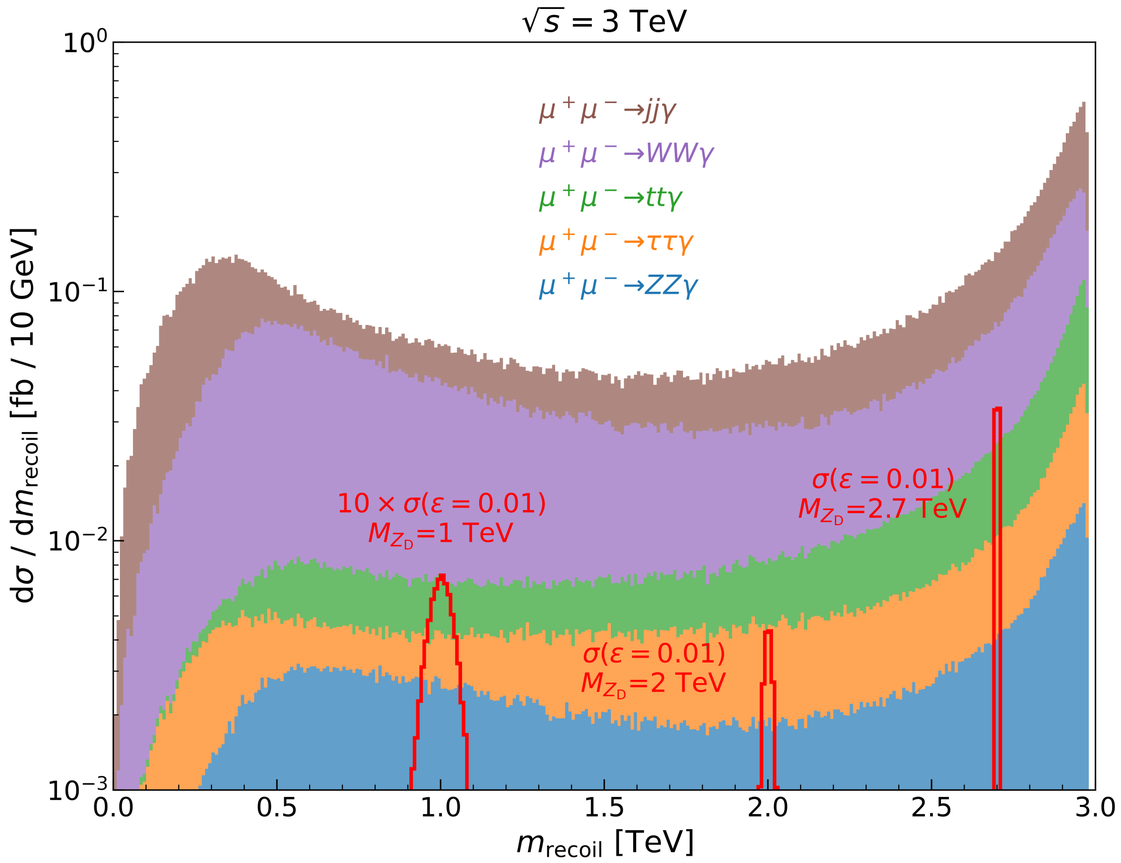

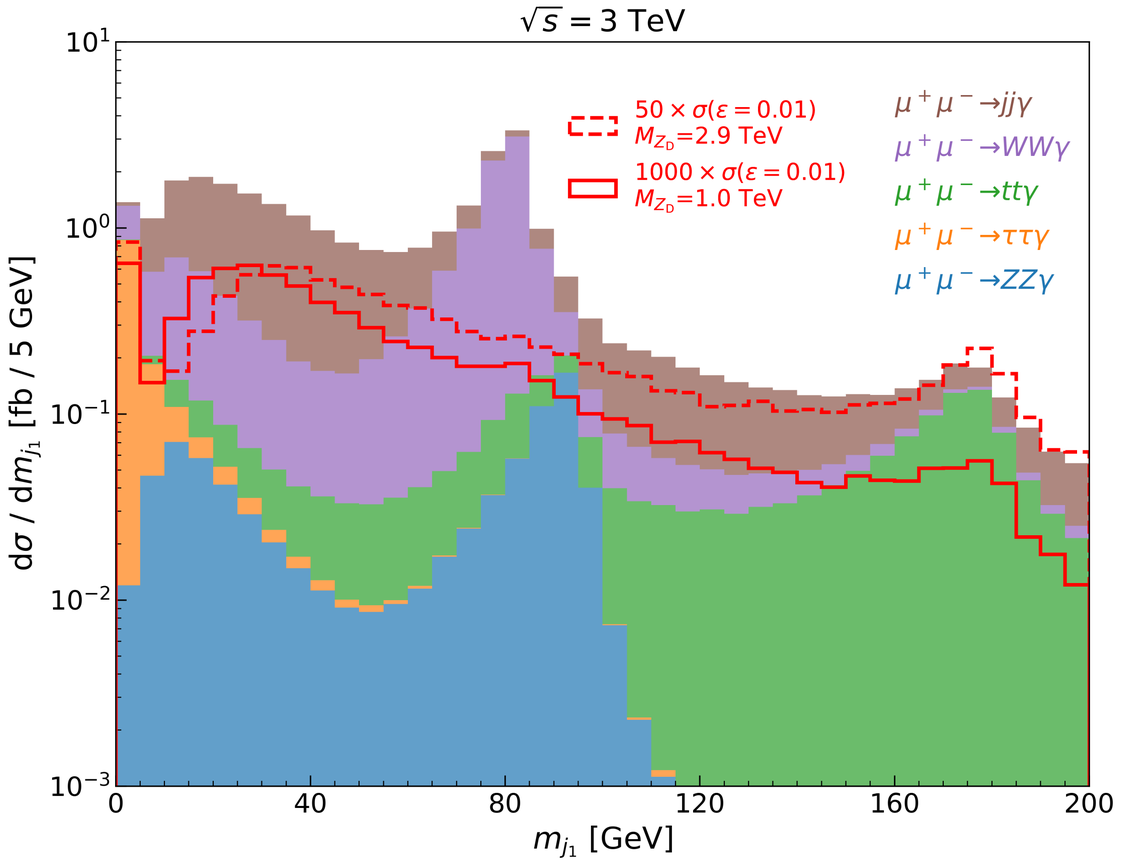

Inclusive Two-Jet Signal Analysis: Distributions

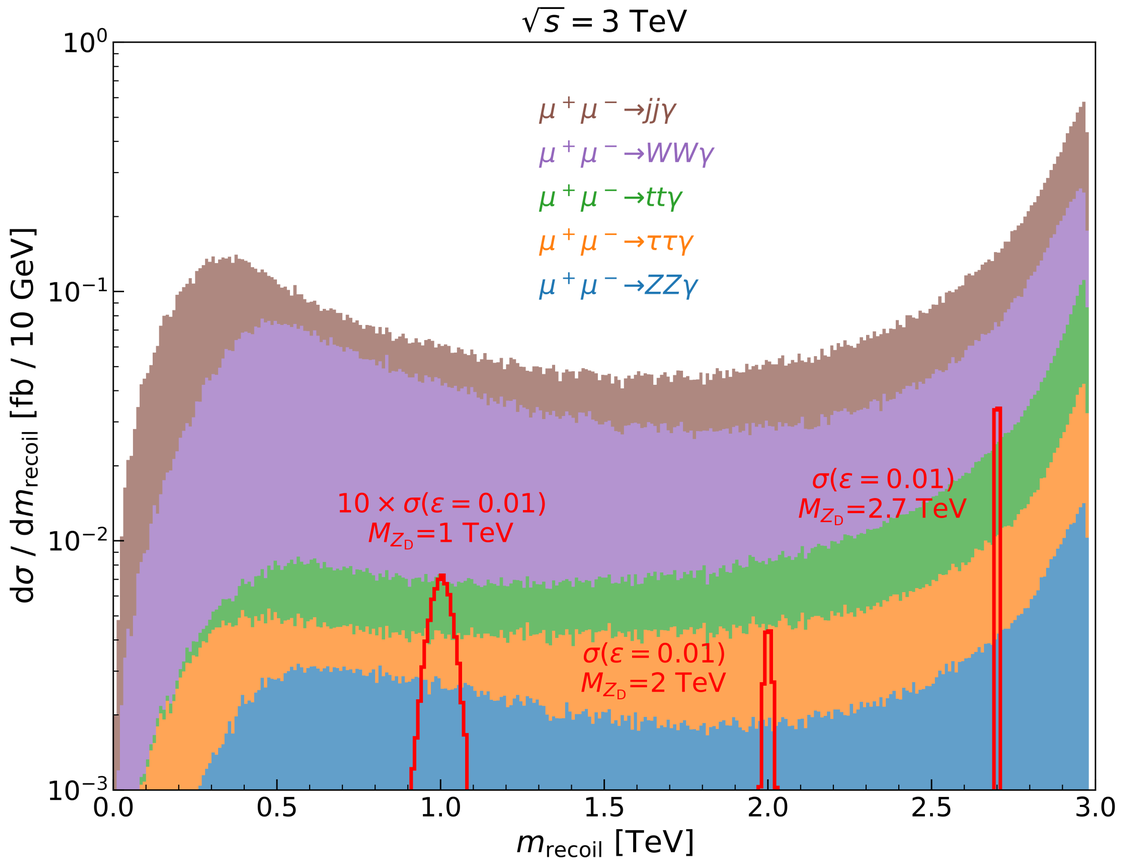

- Over the recoil mass peak, the background distributions are almost flat.
- Narrower peak cut reduces the backgrounds further.

Inclusive Two-Jet Signal Analysis: Distributions

- The leading jet of the backgrounds has a peak in the jet mass distribution.
- If it from the highly collimated two jets decayed from W, in the WWj background.
- We veto the jet mass around m_W.

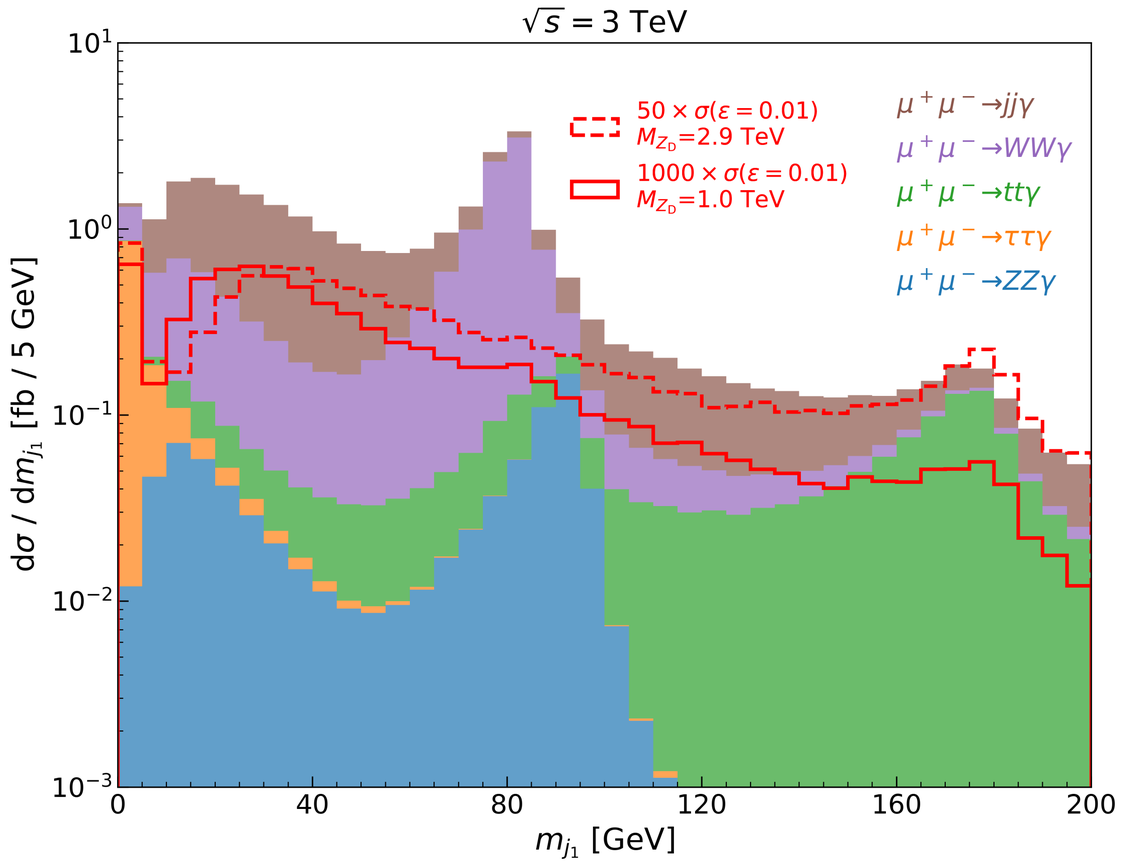

Cut-flow of cross sections (fb) for $\mu^+\mu^- \to Z_{\rm D}(\to jjX)\gamma$ at a 3 TeV MuC with $\mathcal{L}_{\rm tot} = 1\ {\rm ab}^{-1}$						
$M_{Z_{\rm D}} = 1$ TeV & $\varepsilon = 0.01$						
Cut	$Z_{\rm D}(\to jj)\gamma$	$jj\gamma$	$W^+W^-\gamma$	$\tau^+\tau^-\gamma$	$t\bar{t}\gamma$	$\mathcal{S}_{1\,{\rm ab}^{-1}}$
Basic	7.69×10^{-3}	1.42×10	1.15×10	1.08	1.86	2.27×10^{-2}
$\lvert m_{j_1} - m_W\rvert > 20$ GeV	6.34×10^{-3}	1.20×10	3.75	1.08	1.51	4.64×10^{-2}
$\lvert m_{\rm recoil} - M_{Z_{\rm D}}\rvert < 2\Delta m_{\rm recoil}$	3.47×10^{-3}	9.37×10^{-2}	8.47×10^{-2}	1.01×10^{-2}	1.29×10^{-2}	2.41×10^{-1}
$M_{Z_{\rm D}} = 2.7$ TeV & $\varepsilon = 0.01$						
$\lvert m_{\rm recoil} - M_{Z_{\rm D}}\rvert < 2\Delta m_{\rm recoil}$	3.12×10^{-3}	3.32×10^{-2}	6.22×10^{-3}	4.20×10^{-3}	7.72×10^{-3}	4.30

Cut-flow of cross sections (fb) for $\mu^+\mu^- \to Z_{\rm D}(\to jjX)\gamma$ at a 3 TeV MuC with $\mathcal{L}_{\rm tot} = 1\ {\rm ab}^{-1}$						
$M_{Z_{\rm D}} = 1$ TeV & $\varepsilon = 0.01$						
Cut	$Z_{\rm D}(\to jj)\gamma$	$jj\gamma$	$W^+W^-\gamma$	$\tau^+\tau^-\gamma$	$t\bar{t}\gamma$	$\mathcal{S}_{1\,{\rm ab}^{-1}}$
Basic	7.69×10^{-3}	1.42×10	1.15×10	1.08	1.86	2.27×10^{-2}
$\lvert m_{j_1} - m_W\rvert > 20$ GeV	6.34×10^{-3}	1.20×10	3.75	1.08	1.51	4.64×10^{-2}
$\lvert m_{\rm recoil} - M_{Z_{\rm D}}\rvert < 2\Delta m_{\rm recoil}$	3.47×10^{-3}	9.37×10^{-2}	8.47×10^{-2}	1.01×10^{-2}	1.29×10^{-2}	2.41×10^{-1}
$M_{Z_{\rm D}} = 2.7$ TeV & $\varepsilon = 0.01$						
$\lvert m_{\rm recoil} - M_{Z_{\rm D}}\rvert < 2\Delta m_{\rm recoil}$	3.12×10^{-3}	3.32×10^{-2}	6.22×10^{-3}	4.20×10^{-3}	7.72×10^{-3}	4.30

Significance increases greatly via the recoil mass cut, BUT not enough!

Cut-flow of cross sections (fb) for $\mu^+\mu^- \to Z_{\rm D}(\to jjX)\gamma$ at a 3 TeV MuC with $\mathcal{L}_{\rm tot} = 1\ {\rm ab}^{-1}$						
$M_{Z_{\rm D}} = 1$ TeV & $\varepsilon = 0.01$						
Cut	$Z_{\rm D}(\to jj)\gamma$	$jj\gamma$	$W^+W^-\gamma$	$\tau^+\tau^-\gamma$	$t\bar{t}\gamma$	$\mathcal{S}_{1\,{\rm ab}^{-1}}$
Basic	7.69×10^{-3}	1.42×10	1.15×10	1.08	1.86	2.27×10^{-2}
$\lvert m_{j_1} - m_W\rvert > 20$ GeV	6.34×10^{-3}	1.20×10	3.75	1.08	1.51	4.64×10^{-2}
$\lvert m_{\rm recoil} - M_{Z_{\rm D}}\rvert < 2\Delta m_{\rm recoil}$	3.47×10^{-3}	9.37×10^{-2}	8.47×10^{-2}	1.01×10^{-2}	1.29×10^{-2}	2.41×10^{-1}
$M_{Z_{\rm D}} = 2.7$ TeV & $\varepsilon = 0.01$						
$\lvert m_{\rm recoil} - M_{Z_{\rm D}}\rvert < 2\Delta m_{\rm recoil}$	3.12×10^{-3}	3.32×10^{-2}	6.22×10^{-3}	4.20×10^{-3}	7.72×10^{-3}	4.30

Large enough significance mainly because of smaller $\Delta m_{\rm recoil}$ for heavier M_{Z_D}

Cut-flow of cross sections [fb] for $\mu^+\mu^- \to Z_{\rm D}(\to jjX)\gamma$ at a 10 TeV MuC with $\mathcal{L}_{\rm tot} = 10\,{\rm ab}^{-1}$						
$M_{Z_{\rm D}} = 1$ TeV & $\varepsilon = 0.01$						
Cut	$Z_{\rm D}(\to jj)\gamma$	$jj\gamma$	$W^+W^-\gamma$	$\tau^+\tau^-\gamma$	$t\bar{t}\gamma$	$\mathcal{S}_{10\,{\rm ab}^{-1}}$
Basic	5.09×10^{-4}	1.21	1.86	1.37×10^{-1}	2.91×10^{-1}	2.69×10^{-2}
$\lvert m_{j_1} - m_W\rvert > 20$ GeV	4.02×10^{-4}	9.25×10^{-1}	5.14×10^{-1}	1.33×10^{-1}	2.78×10^{-1}	2.93×10^{-2}
$\lvert m_{\rm recoil} - M_{Z_{\rm D}}\rvert < 2\Delta m_{\rm recoil}$	2.28×10^{-4}	4.55×10^{-2}	9.00×10^{-2}	4.49×10^{-3}	9.23×10^{-3}	5.83×10^{-2}
$M_{Z_{\rm D}} = 9.7$ TeV & $\varepsilon = 0.01$						
$\lvert m_{\rm recoil} - M_{Z_{\rm D}}\rvert < 2\Delta m_{\rm recoil}$	1.18×10^{-2}	3.18×10^{-3}	9.43×10^{-4}	3.95×10^{-4}	1.20×10^{-3}	15.5

Cut-flow of cross sections [fb] for $\mu^+\mu^- \to Z_{\rm D}(\to jjX)\gamma$ at a 10 TeV MuC with $\mathcal{L}_{\rm tot} = 10\ {\rm ab}^{-1}$						
$M_{Z_{\rm D}} = 1\ {\rm TeV}\ \ \&\ \ \varepsilon = 0.01$						
Cut	$Z_{\rm D}(\to jj)\gamma$	$jj\gamma$	$W^+W^-\gamma$	$\tau^+\tau^-\gamma$	$t\bar{t}\gamma$	$\mathcal{S}_{10\,{\rm ab}^{-1}}$
Basic	5.09×10^{-4}	1.21	1.86	1.37×10^{-1}	2.91×10^{-1}	2.69×10^{-2}
$\lvert m_{j_1} - m_W\rvert > 20$ GeV	4.02×10^{-4}	9.25×10^{-1}	5.14×10^{-1}	1.33×10^{-1}	2.78×10^{-1}	2.93×10^{-2}
$\lvert m_{\rm recoil} - M_{Z_{\rm D}}\rvert < 2\Delta m_{\rm recoil}$	2.28×10^{-4}	4.55×10^{-2}	9.00×10^{-2}	4.49×10^{-3}	9.23×10^{-3}	5.83×10^{-2}
$M_{Z_{\rm D}} = 9.7\ {\rm TeV}\ \ \&\ \ \varepsilon = 0.01$						
$\lvert m_{\rm recoil} - M_{Z_{\rm D}}\rvert < 2\Delta m_{\rm recoil}$	1.18×10^{-2}	3.18×10^{-3}	9.43×10^{-4}	3.95×10^{-4}	1.20×10^{-3}	15.5

For lighter M_{Z_D}, the 10 TeV MuC is not efficient.

Cut-flow of cross sections [fb] for $\mu^+\mu^- \to Z_{\rm D}(\to jjX)\gamma$ at a 10 TeV MuC with $\mathcal{L}_{\rm tot} = 10\ {\rm ab}^{-1}$						
$M_{Z_{\rm D}} = 1$ TeV & $\varepsilon = 0.01$						
Cut	$Z_{\rm D}(\to jj)\gamma$	$jj\gamma$	$W^+W^-\gamma$	$\tau^+\tau^-\gamma$	$t\bar{t}\gamma$	$\mathcal{S}_{10\,{\rm ab}^{-1}}$
Basic	5.09×10^{-4}	1.21	1.86	1.37×10^{-1}	2.91×10^{-1}	2.69×10^{-2}
$\lvert m_{j_1} - m_W\rvert > 20$ GeV	4.02×10^{-4}	9.25×10^{-1}	5.14×10^{-1}	1.33×10^{-1}	2.78×10^{-1}	2.93×10^{-2}
$\lvert m_{\rm recoil} - M_{Z_{\rm D}}\rvert < 2\Delta m_{\rm recoil}$	2.28×10^{-4}	4.55×10^{-2}	9.00×10^{-2}	4.49×10^{-3}	9.23×10^{-3}	5.83×10^{-2}
$M_{Z_{\rm D}} = 9.7$ TeV & $\varepsilon = 0.01$						
$\lvert m_{\rm recoil} - M_{Z_{\rm D}}\rvert < 2\Delta m_{\rm recoil}$	1.18×10^{-2}	3.18×10^{-3}	9.43×10^{-4}	3.95×10^{-4}	1.20×10^{-3}	15.5

For heavier M_{Z_D}, the 10 TeV MuC is very efficient to probe the dark Z.

3 choices for the mass window cut in ee mode.

Final selection results for $\mu^+\mu^- \to Z_{\mathrm{D}}(\to e^+e^-)\gamma$ at a 3 TeV MuC with $\mathcal{L}_{\mathrm{tot}} = 1\ \mathrm{ab}^{-1}$

	m_{recoil} cut		m_{ee} cut		combined	
	σ_{sig} [fb]	$\mathcal{S}_{1\,\mathrm{ab}^{-1}}$	σ_{sig} [fb]	$\mathcal{S}_{1\,\mathrm{ab}^{-1}}$	σ_{sig} [fb]	$\mathcal{S}_{1\,\mathrm{ab}^{-1}}$
$M_{Z_{\mathrm{D}}} = 1$ TeV	6.01×10^{-4}	1.69×10^{-1}	6.88×10^{-4}	3.88×10^{-1}	3.79×10^{-4}	3.17×10^{-1}
$M_{Z_{\mathrm{D}}} = 2.7$ TeV	5.91×10^{-3}	2.41	5.71×10^{-3}	7.49×10^{-1}	3.23×10^{-3}	1.84

- For lighter M_{Z_D}, m_{ee} cut is more efficient.
- The combined mass window cut is less efficient.

3 choices for the mass window cut in ee mode.

Final selection results for $\mu^+\mu^- \to Z_{\mathrm{D}}(\to e^+e^-)\gamma$ at a 3 TeV MuC with $\mathcal{L}_{\mathrm{tot}} = 1\ \mathrm{ab}^{-1}$

	m_{recoil} cut		m_{ee} cut		combined	
	σ_{sig} [fb]	$\mathcal{S}_{1\,\mathrm{ab}^{-1}}$	σ_{sig} [fb]	$\mathcal{S}_{1\,\mathrm{ab}^{-1}}$	σ_{sig} [fb]	$\mathcal{S}_{1\,\mathrm{ab}^{-1}}$
$M_{Z_{\mathrm{D}}} = 1$ TeV	6.01×10^{-4}	1.69×10^{-1}	6.88×10^{-4}	3.88×10^{-1}	3.79×10^{-4}	3.17×10^{-1}
$M_{Z_{\mathrm{D}}} = 2.7$ TeV	5.91×10^{-3}	2.41	5.71×10^{-3}	7.49×10^{-1}	3.23×10^{-3}	1.84

- For heavier M_{Z_D}, m_{recoil} cut is more efficient.
- The combined mass window cut is less efficient.

ε sensitivity for various M_{Z_D}: inclusive dijet mode

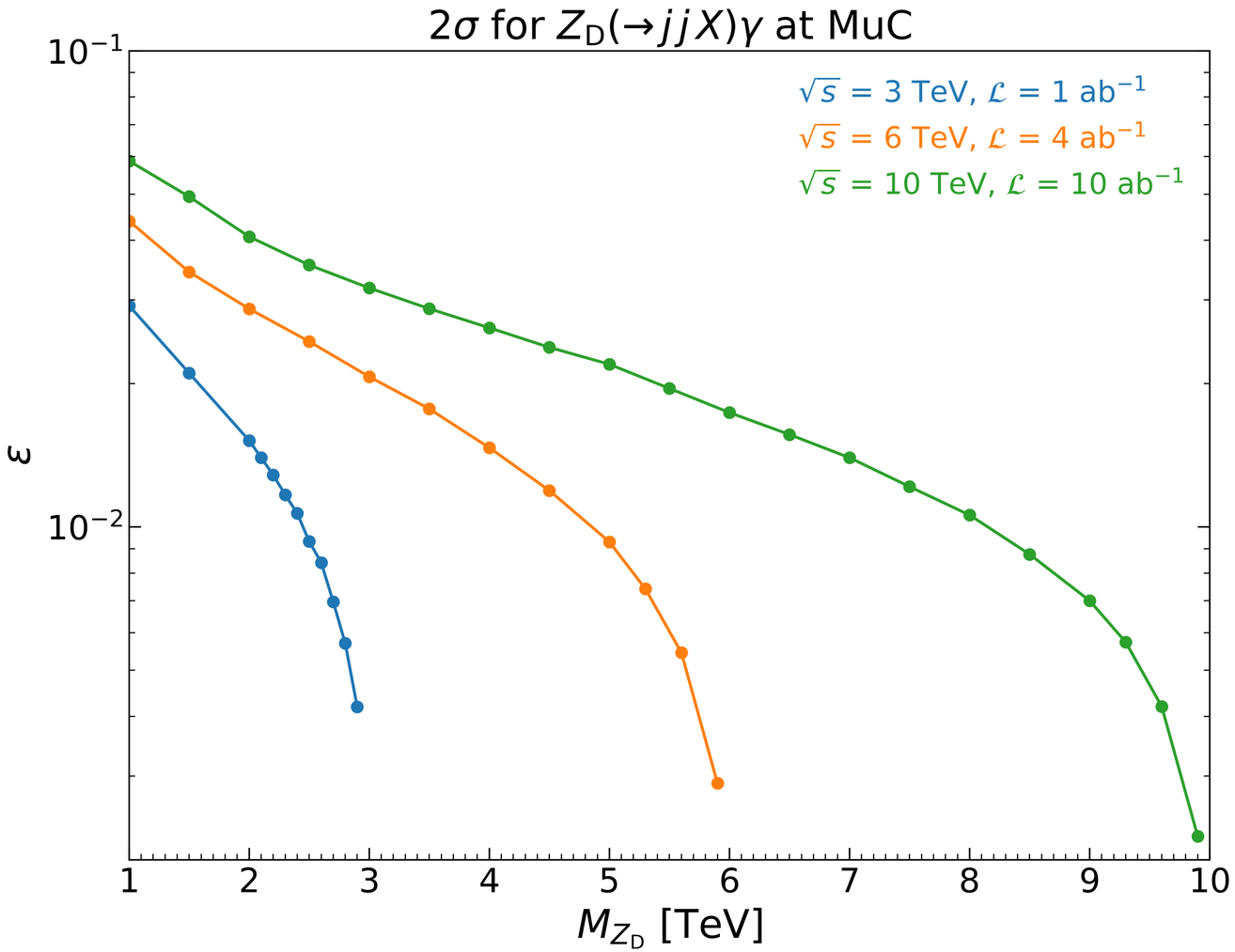

- As M_{Z_D} increase, the ε sensitivity is improved.
- As $\sqrt{s}$, we can probe heavier M_{Z_D} with smaller ε.

ε sensitivity for various M_{Z_D}: ee mode

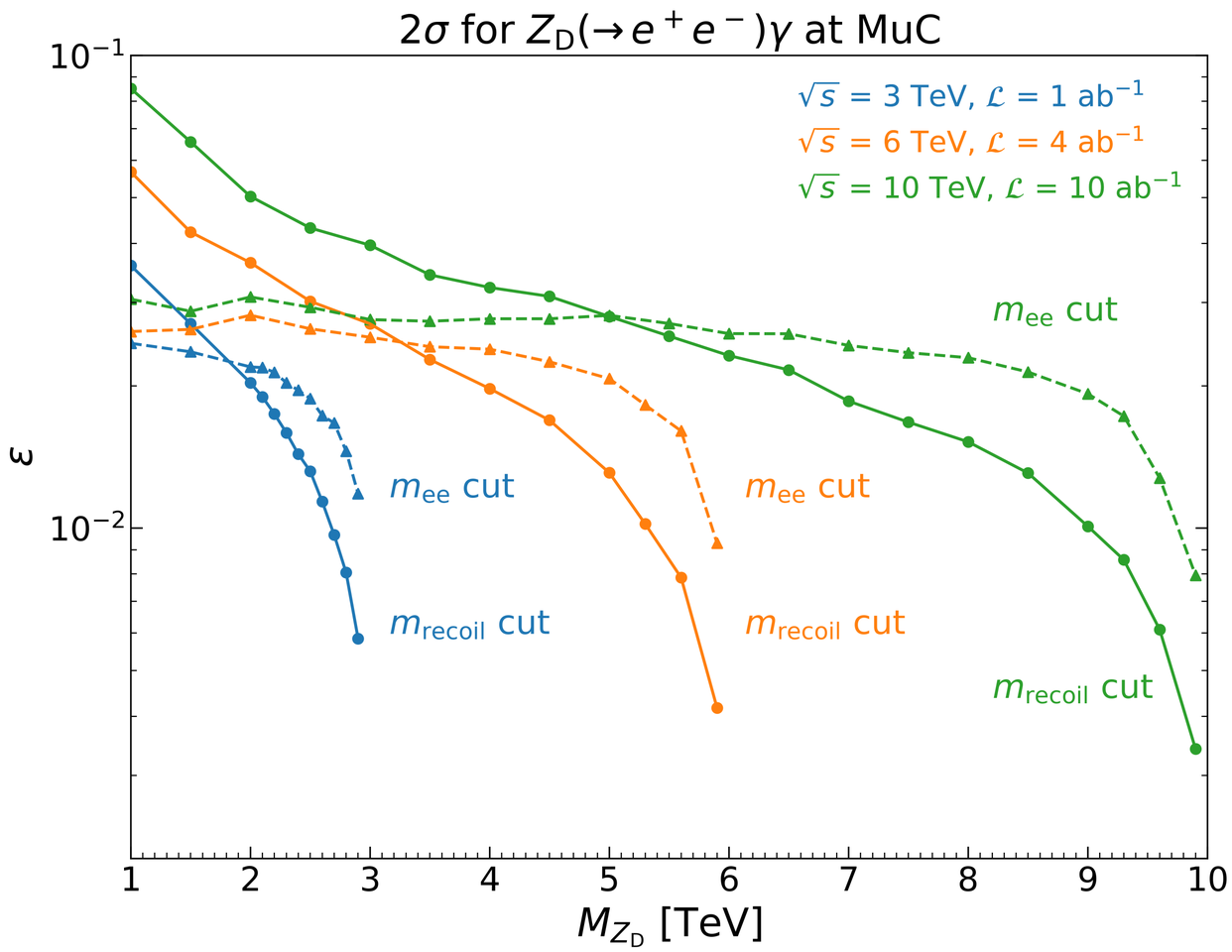

- As M_{Z_D} increase, the εsensitivity is improved.
- As $\sqrt{s}$, we can probe heavier M_{Z_D} with smaller ε.
- m_{ee} cut is efficient for lighter M_{Z_D}, while m_{recoil} is efficient for heavier M_{Z_D}.
- The crossover happens at $M_{Z_D} \simeq \sqrt{s}$.

Combined Sensitivity from jjX and ee

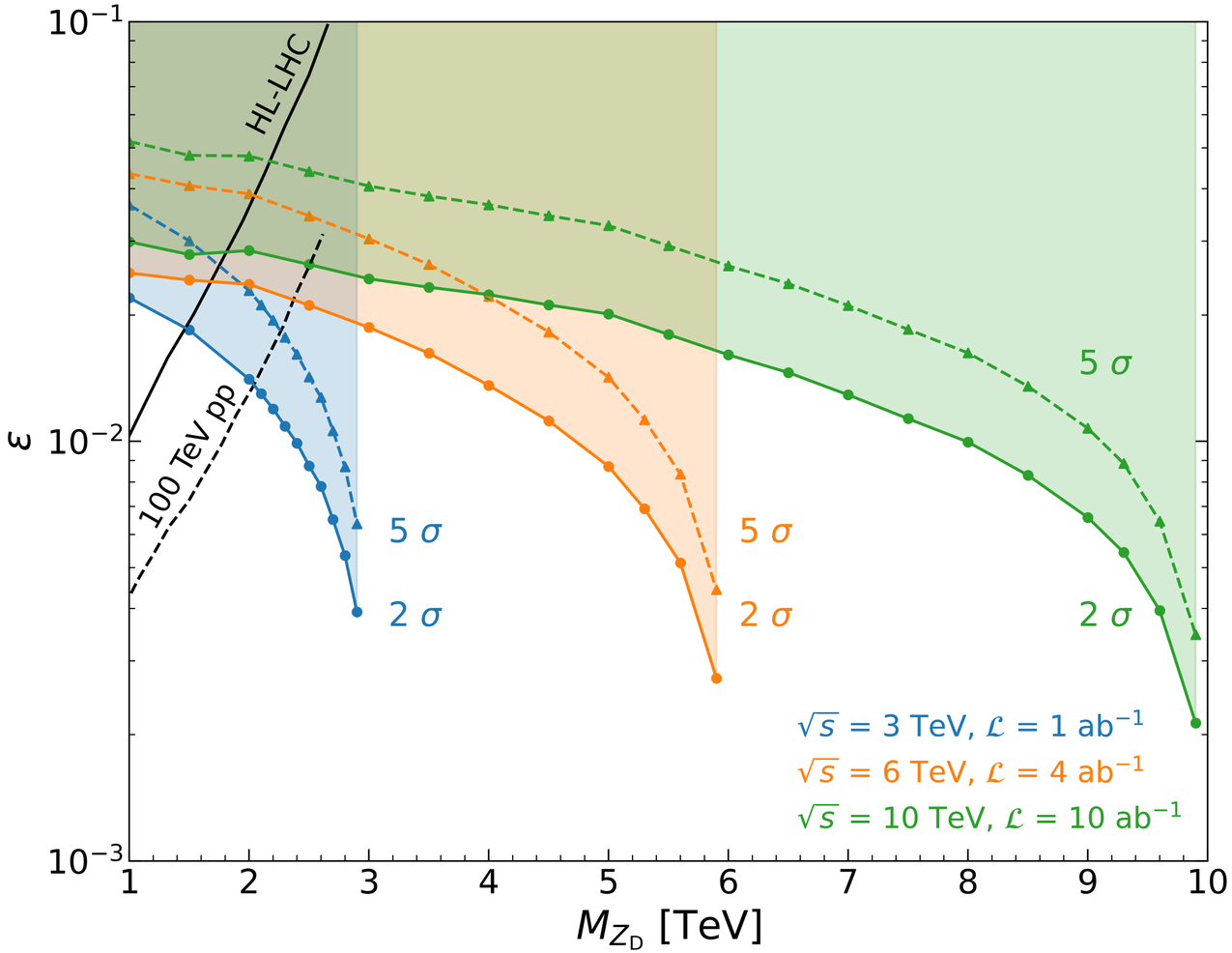

- For $M_{Z_D} > 1.5(2)\,\mathrm{TeV}$, the 3 TeV MuC shows better performance than the HL-LHC (100 TeV pp)
- For $M_{Z_D} \sim \sqrt{s}$, ε sensitivity can reach $\mathcal{O}(10^{-3})$.

VI. Conclusions

- Dark Z is motivated as a potential mediator of interactions between the Standard Model and a hidden dark sector.
- The heavy Z_D is weakly constrained by the current experimental searches, which is more weaker as M_{Z_D} increases.
- The multi-TeV muon colliders can probe the heavy Z_D through the photon associated production with the jjX and ee decay modes, more efficiently for heavier Z_D if we use optimized mass window cuts on m_{recoil} and m_{ee}.